

1 The SAMPL6 SAMPLing challenge: 2 Assessing the reliability and efficiency 3 of binding free energy calculations

4 **Andrea Rizzi**^{1,2*}, **Travis Jensen**³, **David R. Slochower**⁴, **Matteo Aldeghi**⁵, **Vytautas Gapsys**⁵,
5 **Dimitris Ntekoumes**⁶, **Stefano Bosisio**⁷, **Michail Papadourakis**⁷, **Niel M. Henriksen**^{4,8}, **Bert**
6 **L. de Groot**⁵, **Zoe Cournia**⁶, **Alex Dickson**^{9,10}, **Julien Michel**⁷, **Michael K. Gilson**⁴, **Michael R.**
7 **Shirts**³, **David L. Mobley**^{11*}, **John D. Chodera**^{1*}

8 ¹Computational and Systems Biology Program, Sloan Kettering Institute, Memorial Sloan
9 Kettering Cancer Center, New York, NY 10065; ²Tri-Institutional Training Program in
10 Computational Biology and Medicine, New York, NY 10065; ³Department of Chemical and
11 Biological Engineering, University of Colorado Boulder, Boulder, CO 80309; ⁴Skaggs School of
12 Pharmacy and Pharmaceutical Sciences, University of California, San Diego, La Jolla, CA 92093,
13 USA; ⁵Max Planck Institute for Biophysical Chemistry, Computational Biomolecular Dynamics
14 Group, Göttingen, Germany; ⁶Biomedical Research Foundation, Academy of Athens, 4 Soranou
15 Ephessiou, 11527 Athens, Greece; ⁷EaStCHEM School of Chemistry, University of Edinburgh,
16 David Brewster Road, Edinburgh EH9 3FJ, UK; ⁸Atomwise, 717 Market St Suite 800, San Francisco,
17 CA 94103; ⁹Department of Biochemistry and Molecular Biology, Michigan State University, East
18 Lansing, MI, USA; ¹⁰Department of Computational Mathematics, Science and Engineering,
19 Michigan State University, East Lansing, MI, USA; ¹¹Department of Pharmaceutical Sciences and
20 Department of Chemistry, University of California, Irvine, California 92697, USA

21 ***For correspondence:**

22 andrea.rizzi@choderalab.org (AR); dmobley@uci.edu (DLM); john.chodera@choderalab.org (JDC)

24 **Abstract** Approaches for computing small molecule binding free energies based on molecular simula-
25 tions are now regularly being employed by academic and industry practitioners to study receptor-ligand
26 systems and prioritize the synthesis of small molecules for ligand design. Given the variety of methods
27 and implementations available, it is natural to ask how the convergence rates and final predictions of
28 these methods compare. In this study, we describe the concept and results for the SAMPL6 SAMPLing
29 challenge, the first challenge from the SAMPL series focusing on the assessment of convergence properties
30 and reproducibility of binding free energy methodologies. We provided parameter files, partial charges,
31 and multiple initial geometries for two octa-acid (OA) and one cucurbit[8]uril (CB8) host-guest systems.
32 Participants submitted binding free energy predictions as a function of the number of force and energy
33 evaluations for seven different alchemical and physical-pathway (i.e., potential of mean force and weighted
34 ensemble of trajectories) methodologies implemented with the GROMACS, AMBER, NAMD, or OpenMM
35 simulation engines. To rank the methods, we developed an efficiency statistic based on bias and variance
36 of the free energy estimates. For the two small OA binders, the free energy estimates computed with
37 alchemical and potential of mean force approaches show relatively similar variance and bias as a function of
38 the number of energy/force evaluations, with the attach-pull-release (APR), GROMACS expanded ensemble,
39 and NAMD double decoupling submissions obtaining the greatest efficiency. The differences between
40 the methods increase when analyzing the CB8-quinine system, where both the guest size and correlation

41 times for system dynamics are greater. For this system, nonequilibrium switching (GROMACS/NS-DS/SB)
42 obtained the overall highest efficiency. Surprisingly, the results suggest that specifying force field parameters
43 and partial charges is insufficient to generally ensure reproducibility, and we observe differences between
44 seemingly converged predictions ranging approximately from 0.3 to 1.0 kcal/mol, even with almost identical
45 simulations parameters and system setup (e.g., Lennard-Jones cutoff, ionic composition). Further work will
46 be required to completely identify the exact source of these discrepancies. Among the conclusions emerging
47 from the data, we found that Hamiltonian replica exchange—while displaying very small variance—can be
48 affected by a slowly-decaying bias that depends on the initial population of the replicas, that bidirectional
49 estimators are significantly more efficient than unidirectional estimators for nonequilibrium free energy
50 calculations for systems considered, and that the Berendsen barostat introduces non-negligible artifacts in
51 expanded ensemble simulations.

52

53 1 Introduction

54 Predicting the binding free energy between a receptor and a ligand has attracted a great deal of attention
55 due to its potential to speed up small-molecule drug discovery [1]. Among the methodologies that have been
56 developed to carry out this task, physics-based methods employing classical force fields are starting to be
57 routinely used in drug development projects and demonstrate success in real lead optimization scenarios [2–
58 5]. These technologies are also often employed to obtain mechanistic insights into the physics of binding such
59 as the discovery of binding poses [6] and pathways [7], or attempts at providing intuitive guidance on how to
60 improve ligand binding potency [8]. However, the applicability domain of these models is currently limited
61 to a narrow portion of the accessible chemical space for small molecules, and well-behaved protein-ligand
62 systems that do not undergo significant conformational changes or solvent displacement on timescales
63 larger than a few tens of nanoseconds [9, 10]. For this reason, much work has been directed at benchmarking
64 and improving both the predictive accuracy and efficiency of these computational protocols [11–14]. The
65 computational cost of a method, in particular, is a critical factor that enters the decision-making process
66 both in academia and industry. For example, to achieve maximum impact in drug discovery, methods should
67 achieve high-confidence predictions on a timescale sufficiently short to inform synthetic decisions—with
68 increasingly rapid predictions in principle enabling quicker cycles of idea generation and testing. [2, 9, 10].
69 More generally, unconverged results and systematic errors can compromise the assessment of the accuracy
70 of a force field through fortuitous cancellation/amplification of error, with immediate consequences on the
71 optimization of free energy protocols and molecular models. Determining which methods are capable of
72 most rapidly reducing the error is thus critical to enable not only prospective studies in drug discovery, but
73 also to carry out meaningful benchmarks and optimize molecular models with useful turnaround times.

74 1.1 Multiple sources contribute to the error of the estimate

75 In the rest of the work, we refer to the model of the system to include any element affecting the potential
76 energy function we intend to simulate (e.g., force field, charge model, protonation states, ion concentrations).
77 The model, together with the thermodynamic parameters (e.g., temperature, pressure) and the definition
78 of the binding site completely determine the theoretical binding free energy ΔG_θ through the associated
79 ratio of partition functions [15]. The output of a binding free energy method is a statistical estimate of the
80 free energy, a random variable $\Delta G_{\text{calc}} = \Delta G_\theta + \epsilon$, which is an estimate of ΔG_θ up to an error ϵ that generally
81 depends on the method itself and the computational cost invested in the calculation. We consider a method
82 to be efficient if it can quickly reduce the standard deviation of ΔG_{calc} (i.e., $\text{std}(\Delta G_{\text{calc}}) = \text{std}(\epsilon)$) and its bias,
83 which is defined as $\mathbb{E}[\Delta G_{\text{calc}}] - \Delta G_\theta = \mathbb{E}[\epsilon]$, where the expected value is intended over multiple independent
84 executions of the method of the same computational cost.

85 Assuming a method is exact and correctly implemented, the major source of statistical error is arguably
86 connected to the sampling strategy adopted by the method. Due to the rough potential energetic landscape,
87 short molecular dynamics (MD) or Monte Carlo (MC) simulations (where for proteins, short can still be
88 100s of ns) can miss entire areas of configurational space that contribute significantly to the partition

89 functions, or have insufficient time to accurately estimate the relative populations of the different free
90 energy basins. This introduces bias into the affinity estimates. Enhanced sampling strategies such as
91 metadynamics [16, 17], replica exchange [18–20], and expanded ensemble [21] methodologies are designed
92 to increase the sampling efficiency along one or a few collective variables (CV), although their effectiveness
93 strongly depends on the choice of the CV. Moreover, even in the limit of infinite sampling, common non-
94 Metropolisized sampling strategies such as Verlet integration and Langevin dynamics can introduce systematic
95 bias due to the integration error. While the magnitude of this bias has not been studied extensively in free
96 energy calculations of host-guest or protein-ligand systems, it was shown to be significant in simple systems
97 depending on the size of time step, and choice of integrator [22, 23]. Finally, while many different free energy
98 estimators (e.g., exponential averaging, BAR, MBAR, thermodynamic integration) are provably asymptotically
99 unbiased and consistent, these behaviors break down for finite sample sizes, and their bias and variance
100 decay differently as a function of the number of independent samples [24].

101 **1.2 Comparing the efficiency of methods requires eliminating confounding factors**

102 Any simulation parameter altering the potential energy landscape of the end states can alter the energetic
103 barriers between metastable states and change the theoretical binding free energy ΔG_{θ} . The former impact
104 the correlation times of the dynamics and thus the convergence rates of methods, while the latter makes
105 it harder to detect systematic biases introduced by the methodologies. There are several examples in
106 the literature noting differences in binding free energy predictions between different methods, but in
107 which it was impossible to determine whether this was due to other differences in system preparation,
108 insufficient sampling, or shortcomings of the methodology [25–28]. Consequently, it is important to test the
109 methods on the same set of molecular systems, using the same model. The latter, in particular, requires
110 specifying force field parameters and partial charges, but also other components of the simulation, such
111 as ion concentrations and the treatment of long-range interactions (e.g. PME, reaction field, Lennard-Jones
112 cutoff, dispersion correction). Treating long-range interactions equivalently is particularly challenging due to
113 differences in functional forms, implementations, and options supported by the various software packages,
114 including small discrepancies in the value of the Coulomb constant [29, 30]. Establishing a set of simulation
115 settings that minimizes these differences does not prevent systematic bias due to sampling issues, but it
116 makes it possible to detecting by comparing calculations performed with independent methods and/or
117 starting from different initial configurations.

118 Comparing multiple independent methods on the same set of systems currently requires substantial
119 pooled technical expertise and coordination as well as significant computational resources. Confidently
120 estimating the bias necessitates very long simulations and consensus between methods. Moreover, in the
121 absence of a reliable strategy for uncertainty estimation, multiple independent replicates are vital for a
122 correct ranking of performance of different methods. Previous work investigating the reproducibility of
123 relative alchemical hydration free energy calculations across four molecular packages uncovered various
124 issues and challenges in comparing across simulation packages and resulted in various bug fixes [30].
125 However, the reproducibility and efficiencies of various simulation-based approaches has not yet been
126 evaluated in the context of binding free energy calculations, which is the focus of this work.

127 **1.3 We need robust general strategies to measure the efficiency of binding free energy 128 calculations**

129 While there are generally established ways of measuring the accuracy of free energy calculation protocols
130 with respect to experimental measurements, there is no consensus or standard practice regarding how to
131 measure the efficiency of a method. A study focusing on accuracy of free energy calculations typically ranks
132 different protocols and methodologies using commonly adopted correlation and error statistics describing
133 how well experimental affinities are predicted (e.g. R^2 , MUE, and RMSE) [25, 26, 31–34]. On the other hand,
134 the efficiency of sampling strategies in the context of free energy calculations has been evaluated in many
135 different ways in the past, none of which we found completely adequate for the goal of this challenge.

136 In some cases, one or more system-specific collective variables associated with a slow degree of freedom
137 can be directly inspected to verify thorough sampling [27, 35, 36]. This strategy requires extensive knowledge

138 of the system and is not generally applicable to arbitrary receptor-ligand systems. Moreover, free energy
139 calculations commonly involve simulating the same system in multiple intermediate states—which are
140 not always physical intermediates—that do not necessarily have the same kinetic properties. Commonly,
141 quantitative comparisons of performance are based on the standard deviation of the free energy estimates
142 after roughly the same computational cost [37–40]. This statistic, however, does not quantify the bias, which
143 is, in general, not negligible. In principle, one can test the methods on a set of molecules composed of quickly
144 converging systems, or the calculations can be run for a very long time in order to increase our confidence
145 in the assumption that the bias has decayed to zero. However, neither of these two scenarios necessarily
146 reflect the performance of the method in a real scenarios, which ordinarily involves complex receptor-
147 ligand systems with long correlation times and simulations of a few nanoseconds per intermediate state.
148 Alternatively, other statistics such as acceptance rate and mean first-passage time have been reported [39–
149 41], but these statistics are method-specific, and not necessarily indicative of the error of the free energy
150 estimate. Another common strategy to assess the efficiency of a method is the visual inspection of the decay
151 of some error metric [42, 43], but this qualitative analysis is not scalable nor statistically quantifiable when
152 the number of methods and systems considered increases. Finally, there is a large body of theoretical work
153 focusing on the efficiency of estimators and protocols in free energy calculations [24, 37, 40, 42, 44, 45],
154 but in many cases, they are difficult to apply to practical scenarios. The results rely on the assumption of
155 independent samples and often focus on the asymptotic regime, both of which are conditions that may not
156 apply in practice.

157 **1.4 Objectives of the SAMPL6 SAMPLing challenge**

158 In this work, we present the design and the results of the first round of the community-wide **SAMPLing**
159 **challenge**. Our goal is to establish a statistical inference framework for the quantitative comparison of the
160 convergence rates of modern free energy methods on a host-guest benchmark set. Moreover, we assess the
161 level of agreement that can be reached by different methods and software packages when provided identical
162 charges, force field parameters, systems, input geometries, and (when possible) simulation parameters.
163 These objectives are distinct from the goal of the traditional SAMPL host-guest accuracy binding challenge,
164 which instead focuses on the prediction of experimental values and ignores the computational cost of
165 methods. Contrary to the accuracy challenge, which accepted data from widely different methods such as
166 docking [46], QM [47] and QM/MM [48, 49] calculations, or movable type [50, 51] predictions, we limited the
167 scope of this first round of the challenge to force field-based methodologies that should provide identical
168 free energy estimates. With this first round, we lay the groundwork for future SAMPLing challenges and
169 publish a protocol that can be used by independent studies that are similar in scope.

170 **2 Challenge design**

171 **2.1 Selection of the three host-guest systems**

172 The host-guest systems used here are drawn from the SAMPL6 host-guest binding challenge [26]. We
173 selected 5-hexenoic acid (OA-G3) and 4-methylpentanoic acid (OA-G6) as guest molecules of the octa-acid
174 host (OA), and quinine (CB8-G3) for the cucurbit[8]uril (CB8) host (**Figure 1**). The three guests that were
175 chosen for the challenge include molecules resembling typical druglike small molecules (i.e. CB8-G3) and
176 fragments thereof (i.e OA-G3/G6). Quinine was an obvious choice for the former category as it is currently
177 recommended as the second-line treatment for malaria by the World Health Organization [52]. Originally,
178 two octa-acid guests with very similar structures were purposely included to make them easily amenable to
179 relative free energy calculations. However, we did not receive any submission utilizing relative free energy
180 calculations.

181 Both supramolecular hosts have been extensively described in the literature [11, 53–56] and featured in
182 previous rounds of the host-guest binding SAMPL challenge [25, 57, 58]. From the perspective of assessment
183 of binding free energy methodologies, host-guest systems serve as attractive alternatives to protein-ligand
184 systems as they generally do not undergo large conformational reorganizations and have limited number
185 of atoms, which helps the exploration of larger timescales and reducing the uncertainty of the binding

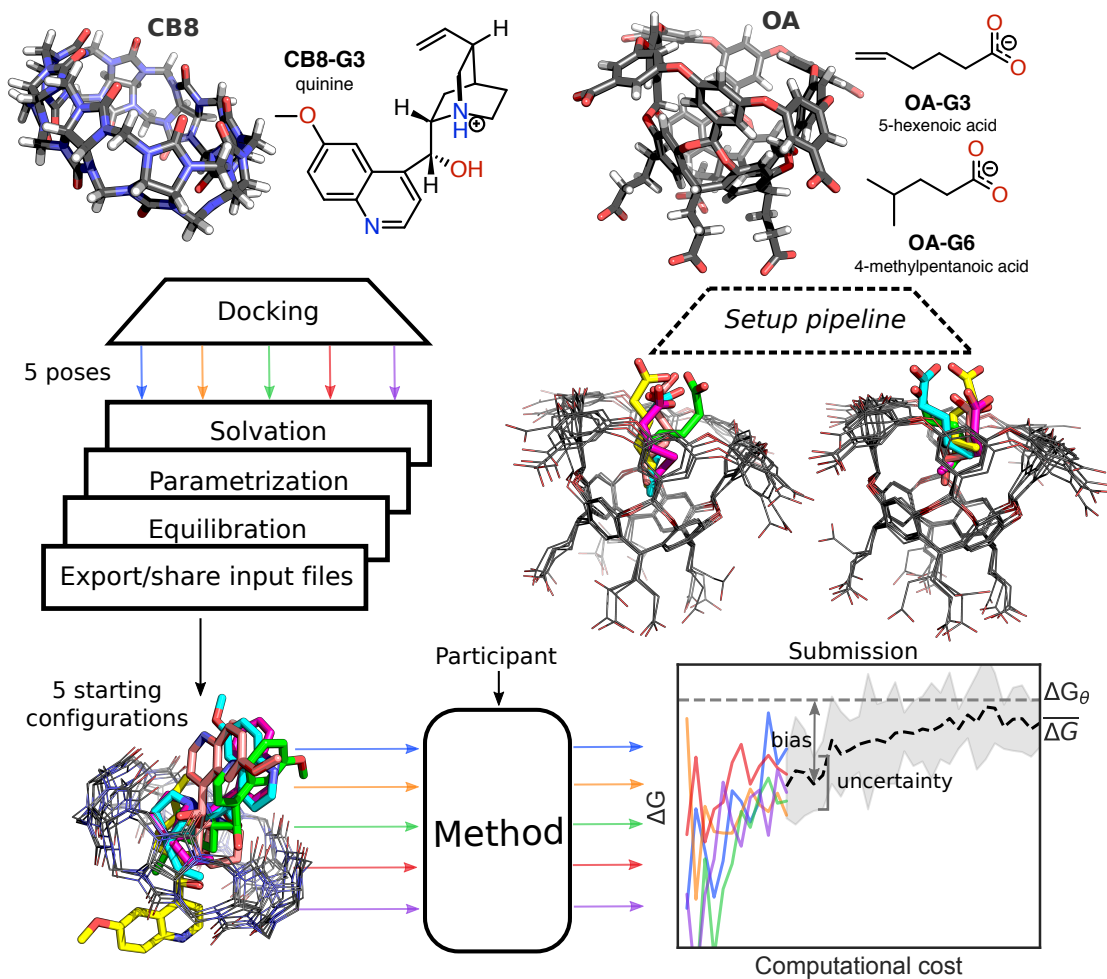


Figure 1. Challenge overview and initial conformations of the host-guest systems featured in the SAMPLing challenge. The three-dimensional structures of the two hosts (i.e. CB8 and OA) are shown with carbon atoms represented in black, oxygens in red, nitrogens in blue, and hydrogens in white. Both the two-dimensional chemical structures of the guest molecules and the three-dimensional structures of the hosts entering the SAMPLing challenge are shown in the protonation state used for the molecular simulations. We generated five different initial conformations for each of the three host-guest pairs through docking, followed by a short equilibration with Langevin dynamics. The three-dimensional structure overlays of the five conformations for CB8-G3, OA-G3, and OA-G6 are shown from left to right in the figure with the guests' carbon atoms colored by conformation. Participants used the resulting input files to run their methods in five replicates and submitted the free energy trajectories as a function of the computational cost. We analyzed the submissions in terms of uncertainty of the mean binding free energy $\overline{\Delta G}$ estimate and its bias with respect to the asymptotic free energy ΔG_θ .

186 affinity estimates. At the same time, this class of systems provides several well-understood challenges
187 for standard simulation techniques. Hosts in the cucurbituril and octa-acid families have been found
188 to bind ions and undergo wetting/dewetting processes governed by timescales on the order of a few
189 nanoseconds [59, 60]. Moreover, the symmetry of CB8 and OA results in multiple equivalent (and often
190 kinetically-separated) binding modes that have to be sampled appropriately or accounted for by applying
191 a correction term [61]. Finally, ligands with net charges can introduce artifacts in alchemical free energy
192 calculations when Ewald methods are used to model long-range electrostatic interactions. There are several
193 approaches for eliminating these errors, but disagreements about the optimal strategy persist [62–65].

194 2.2 Challenge overview

195 As illustrated in *Figure 1*, we asked the participants to run five replicate free energy calculations for each of the
196 three host-guest systems using predetermined force field and simulation parameters and starting from five
197 different conformations that we made available in a GitHub repository ([https://github.com/samplichallenges/
198 SAMPL6/tree/master/host_guest/SAMPLing](https://github.com/samplichallenges/SAMPL6/tree/master/host_guest/SAMPLing)) in the form of input files compatible with common molecular
199 simulation packages (i.e., AMBER, CHARMM, DESMOND, GROMACS, LAMMPS, and OpenMM). Participants
200 were asked to submit binding free energy estimates and, optionally, associated uncertainty estimates as
201 a function of the computational cost of their methodologies. More specifically, the submitted data was
202 required to report 100 free energy estimates computed at regular intervals using the first 1%, . . . , 100% of
203 the samples, which was defined as the amount of samples collected after 1%, . . . , 100% of the combined
204 total number of force and energy evaluations performed for the calculation.

205 To rank the performance of methods, we used a measure of efficiency developed in this work (described
206 in the next section) based on estimates of bias and uncertainty of the predictions obtained from the replicate
207 data. To facilitate the analysis, participants were asked to run the same number of force and energy
208 evaluations for all the five replicate calculations of the same system, although the total number of force
209 and energy evaluations could be different for different systems and different methods. Besides the total
210 number of force and energy evaluations, the submissions included also wall-clock time and, optionally, total
211 CPU/GPU time for each replicate as measures of the computational cost. However, due to the significant
212 differences in the hardware employed to run the simulations, this information was not considered for the
213 purpose of comparing the performance of different methods.

214 2.3 Development of an efficiency statistic for free energy methods

215 In order to rank performance of methods using standard statistical inference tools, we developed a statistic
216 that captures our meaning of efficiency. Unlike what standardly used in the literature (see Section 1.3), we
217 require a measure of the (in)efficiency of a free energy methodology that can simultaneously (1) take into
218 account both bias and variance of the free energy estimate, (2) summarize the performance of a method
219 over a range of computational costs of interest, (3) easily be computed without previous system-specific
220 knowledge (e.g. knowledge of the slowest degrees of freedom).

221 Mean error as an inefficiency statistic

222 In this section, we propose a measure of efficiency of method X based on the time-averaged root mean
223 square error (RMSE) of the binding free energy predicted by method X, ΔG_X , with respect to the theoretical
224 binding free energy determined by the model, ΔG_θ

$$\mathbb{E}_{c_{\min}, c_{\max}}[\text{RMSE}(\Delta G_X(c))] = \frac{\int_{c_{\min}}^{c_{\max}} \text{RMSE}(\Delta G_X(c)) dc}{c_{\max} - c_{\min}} \quad (1)$$

225 where $[c_{\min}, c_{\max}]$ is the range of computational cost of interest, and

$$\text{RMSE}(\Delta G_X(c)) = \sqrt{\mathbb{E}[(\Delta G_X(c) - \Delta G_\theta)^2]} = \sqrt{[\text{std}(\Delta G_X(c))]^2 + [\text{bias}(\Delta G_X(c))]^2} \quad (2)$$

226 where the expected value, standard deviation, and bias functions are intended over all possible realizations
227 (i.e. replicates) of the free energy calculation after investing a computational cost c . This metric satisfies all

228 our requirements. Given the large differences in hardware among the submissions, we chose to measure
229 the computational cost in number of force/energy evaluations rather than CPU or wall-clock time.

More generally, we can consider the *mean error*

$$\mathbb{E}_w[\text{err}(\Delta G_X(c))] = \frac{\int_0^\infty w(c) \text{err}(\Delta G_X(c)) dc}{\int_0^\infty w(c) dc} = 1 \quad (3)$$

where the normalized weight function $w(c)$ can be chosen to limit the average over a finite range of c (i.e. setting $w(c) = 0$ outside some interval), or based on the uncertainty of the estimate of the error statistic err , or also to satisfy other constraints such as the inclination of investing c to obtain a free energy prediction within a workflow. In the analysis, we always chose a uniform weight function as in Eq. (1), but we also report the statistics computed using the standard deviation and absolute bias error functions

$$\begin{aligned} \text{std}(\Delta G_X(c)) &= \sqrt{\mathbb{E}[(\Delta G_X(c) - \mathbb{E}[\Delta G_X(c)])^2]} \\ |\text{bias}(\Delta G_X(c))| &= |\mathbb{E}[\Delta G_X(c) - \Delta G_\theta]| = |\mathbb{E}[\Delta G_X(c)] - \Delta G_\theta| \end{aligned} \quad (4)$$

230 The relative efficiency is a robust statistic when data span different ranges of computational cost
231 The mean error of two methods is sensitive to the interval $[c_{\min}, c_{\max}]$ considered, and thus it can be directly
232 compared only if computed for the same interval of computational cost (see Appendix 1 and SI Figure 4 in
233 the supporting information). However, the calculations submitted by participants have very different lengths,
234 and computing the statistic on the largest range of computational cost shared by all methods would mean
235 discarding between 50% and 75% of the data points for most submissions.

236 Instead, if we have free energy trajectories from a collection of methods A, B, ... spanning different ranges
237 of c , but there is one method Z for which we have data covering the whole range, we can compute the *relative*
238 *efficiency* of all methodologies with respect to Z starting from the ratio of the mean errors

$$e_{\text{err},X/Z} = -\log_{10} \left(\frac{\mathbb{E}_{w_X}[\text{err}(\Delta G_X(c))]}{\mathbb{E}_{w_X}[\text{err}(\Delta G_Z(c))]} \right) = -\log_{10} \left(\frac{\int_{c_{\min,X}}^{c_{\max,X}} \text{err}(\Delta G_X(c)) dc}{\int_{c_{\min,X}}^{c_{\max,X}} \text{err}(\Delta G_Z(c)) dc} \right) \quad (5)$$

239 where err is std, bias, or RMSE, $X = A, B, \dots$, and the weight function w_X is uniform on the interval $[c_{\min,X}, c_{\max,X}]$
240 covered by the data available for method X. The base 10 logarithm ensures $e_{\text{err},X/Z} = -e_{\text{err},Z/X}$ and facilitates
241 interpretation of the statistic: A relative efficiency $e_{X/Z}$ of +1 (-1) means that the total error of X is one order
242 of magnitude smaller (greater) than the total error of Z over the same range of computational cost. We call
243 this the relative *efficiency* of method X as it increases inversely proportional to its mean error. Note that
244 the mean error of Z entering the definition is computed with the same weight function (i.e. over the same
245 interval), which cancels out with the numerator to leave the ratio of the error function areas.

246 If the methods error decay proportionally to the same function of c , the relative efficiency in Eq. (5) is
247 robust to the range of computational cost considered (see Appendix 1 in the supporting information for
248 details). In practice, the statistic seem to be relatively robust to differences in computational cost ranges
249 for most methods (SI Figure 5) with fluctuations that are within the statistical uncertainty of the estimates
250 (SI Figure 6). We thus use the relative efficiency to compare and rank the performance of the methods
251 entering the challenge.

252 **2.4 File preparation and information available to participants**

253 The protocol used to prepare the input files is described in the Detailed Methods section. Briefly, for
254 each host-guest system, five different binding poses were selected among the top-scoring predictions of
255 OpenEye's FRED rigid docking facility [66, 67]. Any docked pose whose guest coordinates had a root mean
256 square deviation (RMSD) less than 0.5 Å with respect to any of the previously accepted docked poses was
257 discarded. This process generated a set of reasonable bound structures with RMSD between any pair of
258 binding poses ranging between 0.72-2.58 Å for CB8-G3 and 1.33-2.01 Å for OA-G3. We then parametrized
259 the systems with AM1-BCC charges [68, 69] and GAFF [70] after solvation in TIP3P [71] water molecules

260 with Na⁺ and Cl⁻ ions added to neutralize the host-guest net charge and reach a 150 mM ionic strength for
261 CB8 and 60 mM for OA-G3/G6. Finally, we relaxed each replicate with 1 ns of Langevin dynamics to obtain
262 the initial conformations shown in **Figure 1**. The five conformations of each host-guest pair generally differ
263 both in their positioning within the symmetric binding site and torsion angles. In particular, all rotatable
264 bonds in the guests adopt at least two different dihedral conformations, with the exception of the bonds
265 connecting the carbon in position 4 in OA-G6 to the two methyl groups, and the two carbon-carbon rotatable
266 bonds composing the secondary alcohol linkage connecting the quinoline moiety and the quinuclidine
267 ring of CB8. The input files for different simulation programs were generated and validated with InterMol.
268 Similarly to what was found in [29], the potential energies computed with different packages for the same
269 structures were generally within 1 kJ/mol from each other, except for those computed with AMBER and
270 CHARMM, which differed by about 2–4 kJ/mol from the others. These results were obtained after tampering
271 with the default settings to make the options as similar as possible. Slightly different Coulomb constants
272 are responsible for approximately 70% of the discrepancies, with AMBER and CHARMM adopting values
273 that are furthest away from each other. The remaining 30% is explained by differences in Lennard-Jones
274 cutoff schemes and PME implementations. The contribution from these differences to binding free energy
275 is not trivial predict, but it is expected to be negligible with respect to statistical error and mostly cancel
276 out at the end states of the thermodynamic cycle. The insensitivity to the Coulomb constant definition
277 and PME parameters was confirmed for Hamiltonian replica exchange calculation with the OA-G3 system
278 (see SI Table 1). A detailed breakdown of the energy components in the different packages can be found
279 at https://github.com/samplchallenges/SAMPL6/tree/master/host_guest/SAMPLing. The input files were
280 uploaded to the public GitHub repository together with details on the setup protocol and general instructions
281 about the challenge (https://github.com/samplchallenges/SAMPL6/blob/master/SAMPLing_instructions.md).
282 The instructions also included the recommended values for the simulation parameters known to affect
283 the theoretical binding free energy (e.g., temperature, pressure, Lennard-Jones cutoff, Particle Mesh Ewald
284 settings) in order to minimize factors that could confound the analysis of systematic differences in free
285 energy predictions between methods.

286 **2.5 Timeline and organization**

287 Initially, the SAMPL6 SAMPLing Challenge was designed as a blind challenge with deadline Jan 19, 2018. This
288 round included data for the methods referred to below as OpenMM/HREX, GROMACS/EE, OpenMM/SOMD,
289 and OpenMM/REVO. However, OpenMM/SOMD and OpenMM/REVO submissions were affected by two
290 trivial bugs in the calculation setup and the analysis respectively that were corrected after the deadline.
291 Moreover, initial disagreement between OpenMM/HREX and GROMACS/EE, which were originally designated
292 to serve as reference calculations to determine eventual systematic biases arising from methodological
293 issues, prompted us to perform additional calculations. For these reasons, and to further increase the
294 opportunities for learning, we elected to extend the study to more methodologies after the initial results of
295 the calculations were made public and to focus the analysis on the non-blind calculations.

296 **3 Results**

297 **3.1 Overview of free energy methodologies entering the challenge**

298 Seven different free energy methodologies based on alchemical or physical binding pathways and imple-
299 mented using AMBER [72], GROMACS [73], NAMD [74], or OpenMM [75] entered the challenge. Four of these
300 (referred to in the following as GROMACS/EE, NAMD/BAR, OpenMM/HREX, and OpenMM/SOMD) used the
301 double decoupling methodology [15], and mainly differ in the enhanced sampling strategies and protocols
302 employed. The other three submissions are based on the potential of mean force (AMBER/APR), alchemical
303 nonequilibrium switching (GROMACS/NS-DS/SB), or weighted ensemble (OpenMM/REVO) frameworks. All of
304 the entries computed standard free energies of binding with respect to a standard concentration of 1 M.

305 In this section, we give a brief overview of the participating free energy methodologies, focusing on
306 their main differences. More details about the methodologies and protocols can be found in Detailed
307 Methods section and in the method description within the submission files available on the public repository

308 at https://github.com/samplchallenges/SAMPL6/tree/master/host_guest/Analysis/Submissions/SAMPLing.
309 Detailed accounts of the results obtained by OpenMM/SOMD and OpenMM/REVO have also been published
310 separately [76, 77] along with detailed accounts of the methodologies they employed.

311 Importantly, in spite of the focus of this challenge on reproducibility and the best efforts of the organizers
312 and participants, small differences in the model, and thus in the theoretical asymptotic free energy of
313 each method, were introduced in the calculations. This was mostly due to fundamental differences in
314 methodologies and software packages. A brief summary of the main differences affecting the models is
315 included at the end of the section.

316 Double decoupling

317 The challenge entries with identifier OpenMM/HREX, GROMACS/EE, NAMD/BAR, and OpenMM/SOMD are
318 based on the double decoupling framework[15] for alchemical absolute free energy calculations, which is
319 arguably the most common approach for current absolute alchemical free energy calculations. All three
320 methodologies estimated free energies and their uncertainties using the multistate Bennet acceptance ratio
321 (MBAR) estimator [78] after decorrelating the data, but they differ mainly in the enhanced sampling strategy
322 (or lack thereof) used to collect the data and details of the protocol employed.

323 OpenMM/HREX used Hamiltonian replica exchange (HREX) [20] to enhance the sampling as implemented
324 in the YANK package [79, 80]. The protocol was based on the thermodynamic cycle in SI Figure 12. Guest
325 charges were annihilated (i.e. intramolecular electrostatic interactions were turned off) before decoupling
326 soft-core Lennard-Jones interactions [81] (i.e. intramolecular interactions were preserved during the al-
327 chemical transformation) between host and guest. Since all guests had a net charge, a randomly selected
328 counterion of opposite charge was decoupled with the guest to maintain box neutrality during the al-
329 chemical transformation. A harmonic restraint between the centers of mass of host and guest was kept
330 active throughout the calculation to prevent the guest to escape the binding site, and the end-points of the
331 thermodynamic cycles were reweighted to remove the bias introduced by the restraint in the bound state by
332 substituting the harmonic restraint potential to a square well potential. Each iteration of the algorithm was
333 composed of Langevin dynamics augmented by Monte Carlo rigid translation and rotation of the guest and
334 by a Hamiltonian global exchange step (i.e. the exchange was not limited to neighbor states) using the Gibbs
335 sampling approach [82]. The pressure was controlled by a Monte Carlo barostat.

336 GROMACS/EE employed the weighted expanded ensemble (EE) enhanced sampling strategy [21]. The
337 calculation was performed in the NVT ensemble, and comprised two separate stages, referred to as equili-
338 bration and production. During equilibration, the Wang-Landau algorithm [83, 84] was used to adaptively
339 converge to a set of expanded ensemble weights that were then used and kept fixed in the production
340 stage. The data generated using the Wang-Landau algorithm is out-of-equilibrium and non-stationary data,
341 so only the samples generated in the production phase were used for the estimation of the free energy
342 through MBAR, which requires equilibrium samples. The equilibration stage was carried out only for a
343 single replicate, and the same equilibrated weights were used to initialize the other four calculations. We
344 analyzed two separate submissions, identified as GROMACS/EE and GROMACS/EE-fullequil, which differ
345 exclusively in whether the computational cost of the equilibration is “amortized” among the 5 replicas (i.e.
346 the cost is added to each replicate after dividing it by 5) or added fully to each of the 5 replicates respectively.
347 The alchemical protocol uses 20 states to annihilate the electrostatic interactions followed by 20 states to
348 annihilate Lennard-Jones. Two restraints attached to the center of mass of host and guest were used in the
349 complex phase: A flat-bottom restraint, which was kept activated throughout the calculation, and a harmonic
350 restraint that was activated during the annihilation of the Lennard-Jones interactions to rigidify the guest
351 in the decoupled state. The Rocklin charge [63] correction was used to remove the effect of the artifacts
352 introduced by alchemically decoupling a molecule with a net charge. The correction amounted to -0.0219
353 and -0.0302 kcal/mol for OA-G3 and OA-G6 respectively.

354 OpenMM/SOMD used the implementation in Sire/OpenMM6.3 [75, 85]. The protocol used 24 interme-
355 diate thermodynamic states for CB8-G3 and 21 states for OA-G3/G6 that were simulated independently
356 (i.e. without enhanced sampling methods) with a velocity Verlet integrator and a 2 femtosecond time-step
357 for 20 ns each and a Monte Carlo barostat. Unlike the other submissions, which constrained only bonds

358 involving hydrogen atoms, here all bonds were constrained to their equilibrium values in the host and guest
359 molecules. The temperature was controlled with an Andersen thermostat [86] set at a collision frequency of
360 10 ps^{-1} , and pressure control was achieved with a Monte Carlo Barostat and isotropic box scaling moves
361 were attempted every 25 time steps. In the complex leg of the calculation, a flat-bottom distance restraint
362 between one atom of the guest and four atoms of the host was kept active throughout the calculation. This
363 is the only submission using a generalization of the Barker-Watts reaction field [87, 88] to model long-range
364 electrostatic interactions instead of Particle Mesh Ewald. Reaction field models usually require larger cutoffs
365 to be accurate for relatively large systems due to the assumption that everything beyond the cutoff can
366 be modeled as a uniform dielectric solvent. Consequently, a 12 Å cutoff was used both for Coulomb and
367 Lennard-Jones interactions instead of the 10 Å cutoff employed by the other methods.

368 Finally, NAMD/BAR calculations were based on the implementation in NAMD 2.12 [74]. In this case as
369 well, the intermediate states were simulated independently with no enhanced sampling strategy and a
370 flat-bottom restraint was used in the complex phase of the calculation. However, 32 λ states were used
371 in which the Lennard-Jones interactions were decoupled in equidistant windows between 0 and 1, and
372 the charges were turned off simultaneously over the λ values 0–0.9 for CB8-G3 and 0–0.5 for OA-G3 and
373 OA-G6. The second schedule was the result of a protocol optimization to work around an issue in which
374 convergence was impaired by a sodium ion binding tightly the carboxylic group of the OA guests in earlier
375 pilot calculations. A non-interacting particle having the same charge as the guest was created during the
376 annihilation of the Coulomb interactions to maintain the charge neutrality of the box. [65, 89]. The system
377 was propagated with Langevin dynamics using a Nosé–Hoover barostat to control the pressure [65, 89]. Free
378 energy estimates and uncertainties were computed with the BAR estimator.

379 Nonequilibrium alchemical calculations

380 In GROMACS/NS-DS/SB, the binding free energies were predicted with alchemical nonequilibrium switching
381 calculations using a strategy referred to previously as double-system/single-box [90]. In this approach, two
382 copies of the guest are simulated in the same box, one of which is restrained to the binding site of the host
383 by a set of restraints as described by Boresch [91]. In addition, a harmonic positional restraint is applied
384 to each of the guest molecules to keep them at a distance of 25 Å from one another. The first guest is
385 decoupled simultaneously with the coupling of the second guest in order to keep the net charge of the box
386 neutral during the alchemical transformation. For each replicate, the calculation was carried out first by
387 collecting equilibrium samples from the two endpoints of the transformation. A total of 50 frames were
388 extracted from each equilibrium simulation at an interval of 400 ps, and each snapshot was used to seed a
389 rapid nonequilibrium alchemical transformation of a fixed duration of 500 ps in both directions. For CB8-G3,
390 a second protocol, here referred to as GROMACS/NS-DS/SB-long, was also applied in which 100 snapshots
391 were extracted from each equilibrium simulation at an interval of 200 ps, and each nonequilibrium trajectory
392 had a duration of 2000 ps. Ten independent calculations were run for each of the 5 initial conformations, and
393 a bi-directional estimator BAR, based on Crook's fluctuation theorem [92], was used to estimate the binding
394 free energy after pooling all work values from all the independent runs. The uncertainty of ΔG for each
395 initial conformation was instead estimated by computing the standard error from the ten independent free
396 energy estimates. Because this approach required two copies of the guest and a box large enough to sample
397 distances between host and guest of 25 Å, the complexes were re-solvated. The force field parameters were
398 taken from the challenge input files. However, both with CB8-G3 and OA-G3/G6, the ion concentration was
399 set to 100 mM, which is different than the reference input files. Unfortunately, we realized this after the
400 calculations were already completed.

401 Potential of mean force

402 AMBER/APR followed the attach-pull-release (APR) [93, 94] methodology to build a potential of mean force
403 profile along a predetermined path of unbinding. The method was implemented in the pAPRika software
404 package based on AMBER [72]. Briefly, the method is divided into three stages. In the “attach” stage, the
405 guest in the binding pocket is gradually rigidified and oriented with respect to the pulling direction in 14
406 intermediate states through the use of 3 restraints. An additional 46 umbrella sampling windows were

407 used to pull the host and guest apart to a distance of 18 Å. A final semi-analytical correction was applied to
408 compute the cost of releasing the restraints and obtain the binding free energy at standard concentration.
409 The analysis was carried out using thermodynamic integration, and the uncertainties were determined using
410 an approach based on blocking and bootstrap analysis. As in the case of GROMACS/NS-DS/SB, the method
411 required larger solvation boxes than the cubic ones provided by the challenge organizers, in order to reach
412 sufficiently large distances between host and guest. Therefore, the initial five complex conformations were
413 re-solvated in an orthorhombic box, elongated in the pulling direction, of TIP3P waters with Na⁺ and Cl⁻ ions.
414 The resulting ionic strength differed from the provided files by about 2–5 mM, but the force field parameters
415 were identical.

416 Weighted ensemble of trajectories

417 The OpenMM/REVO method predicted binding and unbinding kinetic rates with a particular weighted ensemble
418 approach named reweighting of ensembles by variation optimization [77, 95] (REVO) as implemented in
419 the `wepy` package (<https://github.com/ADicksonLab/wepy>) using OpenMM [75]. The calculation was carried
420 out by maintaining a set of 48 independent walkers generating MD trajectories starting from bound and
421 unbound states, the latter defined with a distance between host and guest above 10 Å. At each cycle of the
422 algorithm, some of the walkers are cloned or merged in order to maximize a measure of trajectory variation
423 given by the weighted sum of all-to-all distances between walkers. For unbinding trajectories, the distance
424 between two walkers was defined as the RMSD of the system coordinates after aligning the host, while
425 rebinding trajectories used a measure of distance based on the RMSD with respect to the reference unbound
426 starting structure. The k_{on} and k_{off} rates were estimated directly from the weights of the "reactive" unbinding
427 and rebinding trajectories, and the free energy of binding was computed from the ratio of the rates.

428 Summary of main differences in setups and models

429 While force field parameters and charges were identical in all calculations, there are small differences among
430 the models used by the different methods. The challenge instructions suggested the settings for simulation
431 parameters that are traditionally not included in parameter files. In particular, most calculations were
432 performed at a temperature and pressure of 298.15 K and 1 atm respectively, using particle mesh Ewald
433 (PME) [96] with a cutoff of 10 Å, and employing a Lennard-Jones cutoff of 10 Å with a switching function
434 between 9 Å and 10 Å. Because of methodological and technical reasons, however, not all simulations were
435 run using these settings. In particular, AMBER does not support switching function so AMBER/APR used a 9 Å
436 truncated cutoff instead, and OpenMM/SOMD supports only reaction field for the treatment of long-range
437 electrostatic interactions. Moreover, even when the suggested settings were used, software packages differ
438 in the supported options and parameter values such as PME mesh spacing and spline order, or the exact
439 functional form of the Lennard-Jones switching function. In addition, all the bonds in OpenMM/SOMD were
440 constrained to their equilibrium value, while all the other calculations constrained only the bonds involving
441 hydrogen. Finally, the APR and NS-DS/SB methodologies required a larger solvated box than the cubic one
442 provided by the organizers. Host and guests were thus re-solvated, and while the force field parameters and
443 charges were preserved, the resulting ion concentrations in the box were slightly different from the original
444 files.

445 **3.2 Converged estimates and identical force field parameters do not ensure agreement** 446 **among methods**

447 Absolute free energy calculations can converge to sub-kcal/mol uncertainties in host-guest
448 systems

449 The final predictions of the submitted methods are shown in **Table 1**, **Figure 2**, and SI Figure 7 in terms of
450 the average binding free energy of the five replicate calculations with 95% t-based confidence intervals.
451 With the exception of OpenMM/REVO, the five independent replicate calculations of each method starting
452 from different initial conformations are always within 0.1–0.4 kcal/mol for OA-G3, and 0.1–0.6 kcal/mol for
453 OA-G6 (see also SI Table 3). All methods achieved this level of convergence for the two octa-acid systems
454 in less than $400 \cdot 10^6$ force/energy evaluations (i.e. the equivalent of 800 ns of aggregate MD simulations

455 with a 2 fs integration time step) that can be parallelized over more than 40 processes in all methods
456 with the exception of GROMACS expanded ensemble (see Discussion for more details on parallelization).
457 The agreement between replicates of the same method is generally worse for CB8-G3. Nevertheless, all
458 CB8-G3 predictions of OpenMM/HREX and GROMACS/NS-DS/SB-long are within 0.4 kcal/mol after $2000 \cdot 10^6$
459 force/energy evaluations (i.e. the equivalent of 4 μ s of MD with a 2 fs time step), which suggests that absolute
460 free energy calculations can indeed achieve convergence for this class of systems in reasonable time given
461 widely available computational resources.

462 **Identical force field parameters and charges do not guarantee agreement among methods**
463 Although the predictions of different methods are roughly within 1 kcal/mol, the methods sometimes
464 yield statistically distinguishable free energies. For example, OpenMM/REVO tended towards significantly
465 more negative binding free energies than those predicted by the other methods by about 5-6 kcal/mol,
466 and the final predictions of OpenMM/SOMD for OA-G3 were between 0.5 and 1.0 kcal/mol more positive
467 than the other alchemical and PMF methods. NAMD/BAR and OpenMM/SOMD also generally obtained
468 very negative binding free energies for CB8-G3, but in these two cases, the large statistical uncertainty
469 suggests that the calculations are not close to convergence (i.e. the replicate calculations do not agree).
470 This could be a reflection of the smaller number of energy evaluations used for these submissions (see
471 **Table 1**). AMBER/APR also obtained free energy predictions for OA-G3 and OA-G6 that are significantly
472 different than the predictions from OpenMM/HREX, GROMACS/EE, and NAMD/BAR by 0.2-0.5 kcal/mol.
473 Finally, GROMACS/NS-DS/SB-long and AMBER/APR differ in their predictions for CB8-G3 by 0.8 ± 0.6 kcal/mol.

474 **The origin of the discrepancies between free energy predictions is unclear**
475 In several cases, the interpretation of these results is confounded by differences in simulation parameters
476 and setups. For example, without more data, it is impossible to distinguish whether the systematic bias
477 observed in OpenMM/SOMD is due to sampling issues or the use of reaction field instead of PME or a
478 Lennard-Jones cutoff of 12 Å instead of 10 Å. Multiple explanations are also possible for the other observed
479 discrepancies. Firstly, simulation engines generally differ in the implementation details of the long-range
480 treatment strategies. For example, AMBER does not support switched Lennard-Jones cutoff as the AMBER
481 family of force fields was fit with a truncated cutoff. As a consequence, APR calculations were run using
482 a truncated 9 Å cutoff. In principle, the default values and the algorithms used to determine parameters
483 such as the PME grid spacing and error tolerance can also have an impact on the free energies. Secondly,
484 discrepancies may arise from small differences in the model. Specifically, in order to allow for sufficiently
485 great distances between host and guest in the unbound state, the solvation boxes for APR and NS-DS/SB
486 were regenerated and have a slightly different ionic strength, which is known to affect the binding free
487 energy of host-guest systems. Finally, even for these relatively simple systems, differences in sampling, such
488 as those arising from unsurmounted energetic barriers and different numerical integration schemes, could
489 have affected the convergence of the calculations and introduced non-negligible biases respectively.

490 We investigated most of these hypotheses focusing on APR and HREX, which showed systematic and
491 statistically distinguishable differences of 0.3–0.4 kcal/mol in the final free energies for all systems. The
492 choice of focusing on these two methods was mainly due to technical feasibility as we considered it possible
493 to run further HREX calculations after minimizing the differences in setups and other simulation parameters.
494 However, switching to a truncated 9 Å caused the HREX calculations to increase even further the discrepancies
495 from 0.4 ± 0.1 to 0.7 ± 0.1 , while the HREX calculations resulted insensitive to differences in PME parameters,
496 ionic strength, integrator discretization, Coulomb constant, and restraint employed. Detailed results of the
497 sensitivity analysis of HREX can be found in Appendix 2. Although other explanations exist, it is possible that
498 the observed discrepancies between AMBER/APR and OpenMM/HREX are the results of subtle differences
499 or bugs in the software packages, or of an area of relevant configurational space that is systematically
500 undersampled, which was found to be a problem in host-guest systems both with umbrella sampling [97]
501 and alchemical approaches [98]. A version of APR implemented with OpenMM is close to be completed and
502 might prove useful in determining whether the differences are caused by the methods or the simulation
503 package.

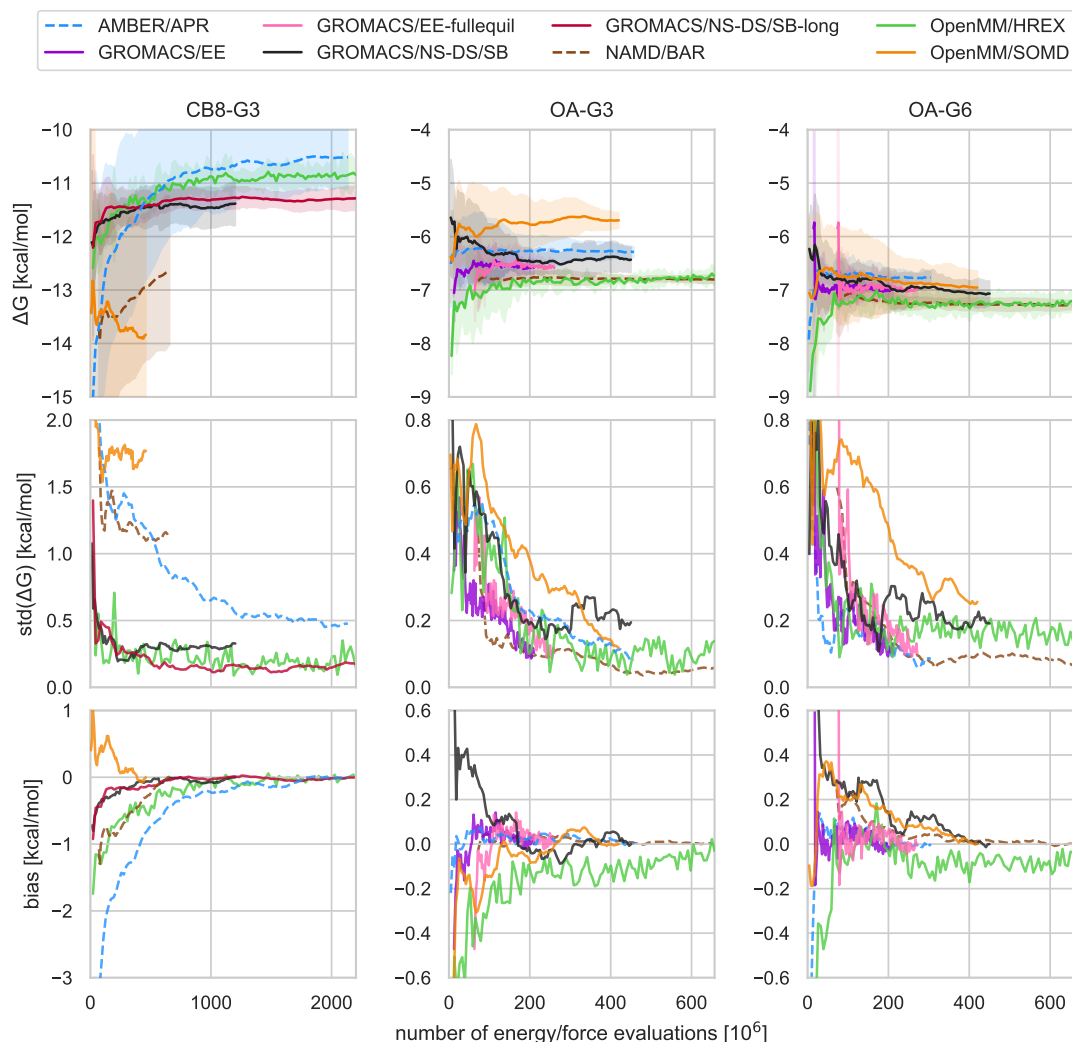


Figure 2. Mean free energy, standard deviation, and bias as a function of computational cost. The trajectories and shaded areas in the top row represent the mean binding free energies and 95% t-based confidence intervals computed from the 5 replicate predictions for CB8-G3 (left column), OA-G3 (center), and OA-G6 (right) for all submissions, excluding OpenMM/REVO. The same plot including OpenMM/REVO can be found in SI Figure 7. The second and third rows show the standard deviation and bias, respectively, as a function of the computational effort. Given the differences in the simulation parameters between different methods, the finite-time bias is estimated assuming the theoretical binding free energy of the calculation to be the final value of its mean free energy. This means that the bias eventually goes to zero, but also that the bias can be underestimated if the simulation is not converged.

504 Further work will be required to establish the exact source of the persistent deviation between seemingly
 505 well-converged calculations.

506 3.3 Bias and variance of free energy estimates can vary greatly with methods and 507 protocols

508 We estimated standard deviation, bias, and RMSE relative efficiencies for all methods and built bias-corrected
 509 and accelerated (BCa) bootstrap [99] 95% confidence intervals (see also Detailed Methods for details). We
 510 used the total combined number of force and energy evaluations to measure the computational cost, and
 511 OpenMM/HREX was used as a reference for the calculation of the relative efficiencies because it was the
 512 longest calculation and could thus provide free energy estimates for all the computational cost intervals
 513 required to estimate the statistics. The resulting relative efficiencies with confidence intervals are represented

Table 1. Average binding free energy predictions, computational cost, and relative efficiencies of all methods.

Final average binding free energy predictions in kcal/mol computed from the five independent replicate calculations with 95% t-based confidence intervals. The computational cost is reported in millions of force and energy evaluations per replicate calculation. Relative efficiencies of a method X are reported with respect to OpenMM/HREX as $e_{\text{err},X}/\text{OpenMM/HREX}$ as defined by Eq. (5). The lower and upper bound of the 95% confidence intervals bootstrap estimates for the relative efficiencies are reported as subscript and superscript respectively.

Method	CB8-G3					OA-G3					OA-G6				
	ΔG [kcal/mol]	n_{eval} [$\times 10^6$]	e_{std}	e_{bias}	e_{RMSE}	ΔG [kcal/mol]	n_{eval} [$\times 10^6$]	e_{std}	e_{bias}	e_{RMSE}	ΔG [kcal/mol]	n_{eval} [$\times 10^6$]	e_{std}	e_{bias}	e_{RMSE}
AMBER/APR	-10.5 ± 0.6	2135	-0.6 ^{-0.4} _{-0.9}	-0.4 ^{0.0} _{-0.8}	-0.5 ^{-0.1} _{-0.6}	-6.3 ± 0.1	458	-0.1 ^{0.1} _{-0.3}	0.7 ^{0.9} _{0.5}	0.0 ^{0.2} _{-0.2}	-6.8 ± 0.1	305	0.1 ^{0.3} _{0.0}	0.35 ^{0.47} _{0.28}	0.2 ^{0.3} _{0.1}
GROMACS/EE						-6.6 ± 0.1	210	0.2 ^{0.8} _{0.0}	0.5 ^{0.7} _{0.2}	0.3 ^{0.5} _{0.1}	-7.0 ± 0.1	212	-0.1 ^{0.1} _{-0.2}	0.32 ^{0.39} _{0.27}	0.01 ^{0.09} _{0.02}
GROMACS/EE-fullequil						-6.6 ± 0.1	261	0.05 ^{0.52} _{0.04}	0.5 ^{0.7} _{0.3}	0.2 ^{0.4} _{-0.1}	-7.0 ± 0.1	271	-0.2 ^{0.2} _{-0.3}	0.0 ^{0.4} _{-0.2}	-0.1 ^{0.1} _{-0.3}
GROMACS/NS-DS/SB	-11.4 ± 0.4	1202	-0.1 ^{0.1} _{-0.3}	0.5 ^{0.8} _{0.2}	0.2 ^{0.3} _{0.0}	-6.4 ± 0.2	450	-0.1 ^{0.0} _{-0.2}	0.1 ^{0.3} _{-0.2}	0.06 ^{0.00} _{-0.17}	-7.1 ± 0.2	450	-0.1 ^{0.2} _{-0.3}	-0.2 ^{0.1} _{-0.5}	-0.1 ^{0.1} _{-0.3}
GROMACS/NS-DS/SB-long	-11.3 ± 0.2	2202	0.2 ^{0.2} _{-0.1}	0.5 ^{0.8} _{0.4}	0.25 ^{0.32} _{0.21}										
NAMD/BAR	-13.0 ± 1.0	657	-0.8 ^{-0.2} _{-0.9}	0.2 ^{0.7} _{-0.3}	-0.18 ^{0.08} _{-0.40}	-6.8 ± 0.07	657	0.2 ^{0.5} _{0.0}	0.9 ^{1.1} _{0.7}	0.4 ^{0.5} _{0.1}	-7.28 ± 0.08	657	0.1 ^{0.3} _{-0.4}	0.3 ^{0.6} _{-0.3}	0.1 ^{0.3} _{-0.2}
OpenMM/REVO	-16.0 ± 1.0	1920	-1.1 ^{-0.9} _{-1.3}	-0.9 ^{-0.6} _{-1.3}	-1.0 ^{-0.7} _{-1.3}	-11.0 ± 2.0	1920	-1.3 ^{-1.1} _{-1.5}	-1.4 ^{-0.8} _{-1.8}	-1.4 ^{-1.0} _{-1.6}	-12.0 ± 1.0	1920	-1.3 ^{-1.1} _{-1.7}	-1.9 ^{-1.7} _{-2.1}	-1.50 ^{-1.42} _{-1.66}
OpenMM/SOMD	-14.0 ± 2.0	460	-0.8 ^{-0.2} _{-1.0}	0.5 ^{0.8} _{0.3}	-0.3 ^{0.0} _{-0.5}	-5.7 ± 0.1	420	-0.2 ^{0.0} _{-0.5}	0.2 ^{0.6} _{-0.1}	-0.1 ^{0.1} _{-0.3}	-7.0 ± 0.3	420	-0.3 ^{0.0} _{-0.5}	-0.1 ^{0.3} _{-0.6}	-0.3 ^{0.1} _{-0.4}
OpenMM/HREX	-10.8 ± 0.2	3327	0.0	0.0	0.0	-6.71 ± 0.05	2789	0.0	0.0	0.0	-7.18 ± 0.06	2615	0.0	0.0	0.0

514 in **Table 1**.

515 The methods displayed system-dependent performance

516 Overall, no method emerged as a superior choice in all three systems, but double decoupling, potential of
517 mean force, and nonequilibrium switching all proved to be solid approaches to obtained precise binding
518 free energy estimates for the host-guest systems considered. Indeed, GROMACS/NS-DS/SB (nonequilibrium
519 switching with double-system/single box), NAMD/BAR (double decoupling), and AMBER/APR (potential of
520 mean force) obtained the greatest RMSD efficiency for CB8-G3, OA-G3, and OA-G6 respectively. In general,
521 however, all methods showed larger uncertainty and slower convergence for CB8-G3 than for OA-G3/G6
522 (Figure 2), and the differences among the methods' performance, which were relatively small for the two
523 octa-acid systems, increased for CB8-G3. For example, with GROMACS/EE, it was not possible to equilibrate
524 the expanded ensemble weights within the same time used for OA-G3/G6. Moreover, OpenMM/SOMD
525 and NAMD/BAR replicate calculations could not converge the average free energy to uncertainties below
526 1 kcal/mol, and OpenMM/HREX and AMBER/APR displayed a significant and slowly decaying bias. Contrarily,
527 GROMACS/NS-DS/SB, which generally obtained a slightly negative relative efficiency in OA-G3/G6, performed
528 significantly better than any other methods with CB8-G3 and obtained variance similar to OpenMM/HREX
529 but smaller total bias.

530 Enhanced-sampling strategies can increase convergence rates in systems with long correlation
531 times

532 The four double decoupling methods performed similarly for the two octa-acid systems, while differences
533 in performance widened with CB8-G3, which featured the largest guest molecule in the set and generally
534 proved to be more challenging for free energy methods than OA-G3/G6. OpenMM/HREX obtained much
535 smaller uncertainties and bias with CB8-G3 than both OpenMM/SOMD and NAMD/BAR, whose replicates
536 seem far from converging to a single prediction. Looking at the individual replicate free energy trajectories
537 for CB8-G3 (SI Figure 9), one notices that both OpenMM/SOMD and NAMD/BAR produced a few relatively
538 flat trajectories that differ by 3-4 kcal/mol. Further OpenMM/SOMD repeats suggest that the replicate
539 disagreement is not determined by the initial conformations, and it is more likely caused by long mixing
540 times of the system (SI Table 5). The difference in performance with respect to OpenMM/HREX for CB8-G3
541 might then be explained by the Hamiltonian replica exchange strategy, which is in agreement with previous
542 studies on cucurbit[7]uril [100]. On the other hand, NAMD/BAR and GROMACS/EE obtained the greatest
543 relative efficiencies for OA-G3/G6, and, while their difference in efficiency is not statistically significant, it is

544 worth noticing that NAMD/BAR did not employ enhanced sampling methodologies. This suggests that the
545 impact of enhanced sampling strategies based on Hamiltonian exchange might be significant in absolute
546 free energy calculations only for transformations and systems with long correlation times.

547 Nonequilibrium switching trajectories (the NS protocol) also seemed to be effective in working around
548 problematic energetic barriers in CB8-G3 associated with the alchemical transformation. In particular,
549 NS-DS/SB-long, which used longer nonequilibrium switching trajectories, slightly improved the efficiency of
550 the method in CB8-G3. This suggests that collecting fewer nonequilibrium switching trajectories to achieve a
551 narrower nonequilibrium work distribution can be advantageous in some regimes.

552 As a final note, NAMD/BAR generally obtained a greater efficiency than OpenMM/SOMD in OA-G3/G6,
553 which also did not use any enhanced sampling approach. It is unclear whether this difference is due to
554 the number of intermediate states (32 for NAMD/BAR, 21 for OpenMM/SOMD), the initial equilibration of
555 2 ns performed by NAMD/BAR, or the long-range electrostatics model (PME for NAMD/BAR and reaction
556 field for OpenMM/SOMD). It is clear, however, that two different but reasonable protocols can result in very
557 different efficiencies. As a confirmation of this, the NAMD/BAR submission for OA-G3/G6 used an optimized
558 λ schedule turning off charges linearly between λ values 0.0–0.5 rather than 0.0–0.9 as done in the first batch
559 of calculations. The new λ schedule considerably improved the convergence over the original protocol, which
560 was causing long mixing times due to sodium ions binding tightly the carboxylic group of the OA guests.

561 Equilibrating expanded ensemble weights can increase efficiency when running replicates
562 In the two octa-acid systems, OpenMM/HREX and GROMACS/EE-fullequil achieved similar efficiencies,
563 although the latter obtained a better absolute bias relative efficiency with OA-G3. GROMACS/EE obtained,
564 however, a greater RMSE relative efficiency when the cost of equilibrating the expanded ensemble weights
565 is amortized over the five replicate calculations. This strategy is thus attractive when precise uncertainty
566 estimates through replicate calculations are required. These observations, however, are limited to the
567 two OA systems as the expanded ensemble weights equilibration stage did not converge in sufficient time
568 for CB8-G3. Finally, we note that differences in the details of the protocols between GROMACS/EE and
569 OpenMM/HREX may explain the greater efficiency of the former.

570 In the expanded ensemble strategy, the weights attempt to bias the probability of jumping from a state
571 to another in order to sample all intermediate states equally. In the presence of bottlenecks, this helps
572 to reduce the round trip time along the alchemical λ variable, which in turn can help reducing correlation
573 times of the sampled binding poses in the bound state. Moreover, while OpenMM/HREX decoupled a
574 counterion of opposite charge to the guest to maintain the neutrality of the simulation box, GROMACS/EE
575 corrected for Coulomb finite-size effects arising with PME using an analytical correction [63]. While the
576 approach decoupling the counterion does not introduce approximations, the process of discharging an ion
577 is accompanied by solvent reorganization, which could impact the statistical efficiency of the calculation.
578 Finally, GROMACS/EE annihilated Lennard-Jones (LJ) interactions (i.e. intra-molecular LJ forces were turned
579 off in the decoupled state) while OpenMM/HREX decoupled them (i.e. intra-molecular LJ interactions were
580 left untouched). The choice of decoupling versus annihilating has two effects on convergence, and these
581 may work in opposite directions. On one hand, annihilating the LJ could increase the thermodynamic length
582 of the transformation, which was found to be directly connected to the minimum theoretical variance of the
583 free energy estimate [40]. On the other hand, annihilation of internal LJ interactions might remove some
584 energy barriers separating metastable states, which could help reducing correlation times.

585 Estimating binding free energies via estimation of binding kinetics was an order of magnitude
586 less efficient than predicting binding free energies directly
587 OpenMM/REVO employed a dramatically different approach for free energy prediction, calculating estimates
588 of the binding kinetics through direct sampling of the binding and unbinding processes. The free energies
589 obtained using the ratio of the binding and unbinding rates had larger uncertainties and showed a significant
590 systematic bias with respect to other methodologies, although the ranking of the compounds agrees with
591 the other submissions. The slow unbinding process may be responsible for the large variance and bias
592 observed in REVO. Indeed, REVO calculations collected a total of 1.92 μ s per system per replicate, which

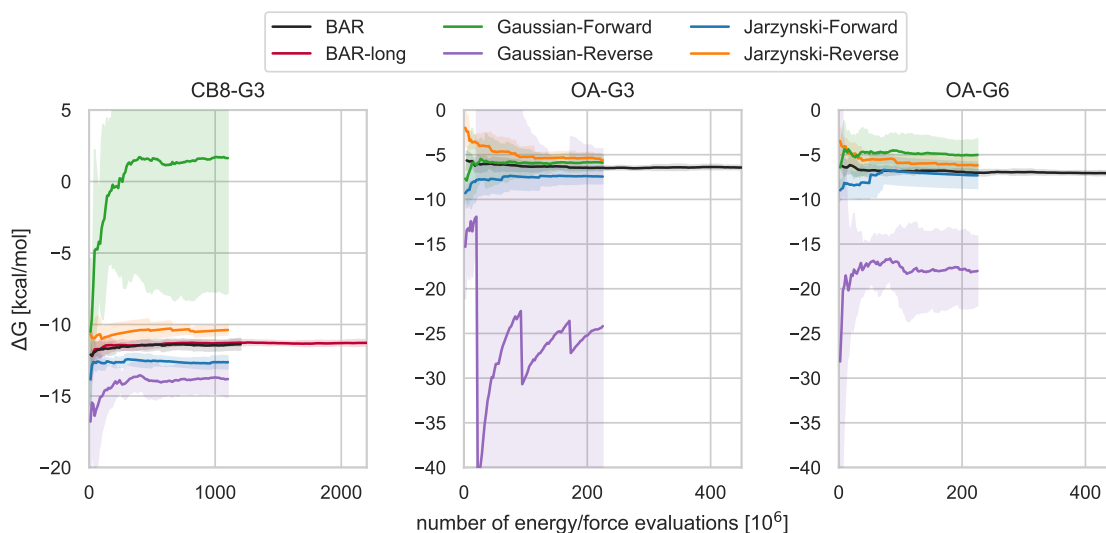


Figure 3. Comparison of bidirectional and unidirectional free energy estimators of the same nonequilibrium work switching data. Average free energy estimates obtained by different estimators from the same nonequilibrium work data collected for CB8-G3 (left), OA-G3 (center), and OA-G6 (right) as a function of the number of energy/force evaluations. The average and the 95% t-based confidence interval (shaded areas) are computed from the 5 replicate calculations. BAR and BAR-long correspond to the GROMACS/NS-DS/SB and GROMACS/NS-DS/SB-long submissions in *Figure 2*, and utilize the bidirectional Bennett acceptance ratio estimator based on the Crooks fluctuation theorem [101]. Jarzynski-Forward/Reverse are the free energy estimates computed through unidirectional estimators derived from the Jarzynski equality using only the nonequilibrium work values accumulated in the forward/reverse direction respectively. The Gaussian-Forward/Reverse trajectories are based on the Crooks fluctuation theorem and the assumption of normality of the forward/reverse nonequilibrium work distribution, as described in [102]. Unidirectional estimators can introduce significant instabilities and bias in the estimates.

593 should allow obtaining reasonably robust statistics for the binding process, whose mean first passage time
594 (MFPT) estimated by the method for the three systems was between 36 ± 6 and 150 ± 50 ns [77]. On the other
595 hand, the MFPT estimates for the unbinding process yielded by the method were $6 \pm 4 \mu\text{s}$ for OA-G3, 2.1 ± 0.5 s
596 for OA-G6, and 800 ± 200 s for CB8-G3, which is significantly beyond the reach of the data accumulated for
597 the prediction, and suggests that further simulation is required to obtain a better estimate of k_{off} and ΔG .
598 Another possible element that may have affected the asymptotic free energies is the size of the simulation
599 box, which was relatively small for this type of calculation and made it difficult to sample long distances
600 between host and guest in the unbound state, which can artificially lower the unbinding rate. Despite the
601 smaller efficiency in predicting the binding free energy, this method was the only one among the submissions
602 capable of providing information on the kinetics of binding.

603 **3.4 Unidirectional nonequilibrium work estimators can be heavily biased and** 604 **statistically unstable**

605 We verified how the choice of the estimator can impact the convergence of the free energy estimate in
606 nonequilibrium switching calculations. In particular, besides the bi-directional BAR estimates discussed
607 above (GROMACS/NS-DS/SB and GROMACS/NS-DS/SB-long), we computed binding free energies of the host-
608 guest systems using uni-directional estimator based on Jarzynski's equality [103] in both forward and reverse
609 directions and the estimator presented in [102], which is based on Jarzynski's equality and the assumption
610 of normality of the nonequilibrium work distribution. No extra simulation was run to obtain these new
611 estimates. Rather, the same nonequilibrium data produced by the GROMACS/NS-DS/SB and GROMACS/NS-
612 DS/SB-long protocols were re-analyzed using the unidirectional estimators. Their associated computational
613 cost was halved to account for the fact that the method required to generate only nonequilibrium switching
614 trajectories in one direction. As can be seen in *Figure 3* and in SI Table 3, the efficiency of unidirectional
615 estimators is significantly smaller than one obtained with BAR in all cases but GROMACS/NS-Jarz-F for OA-G3,

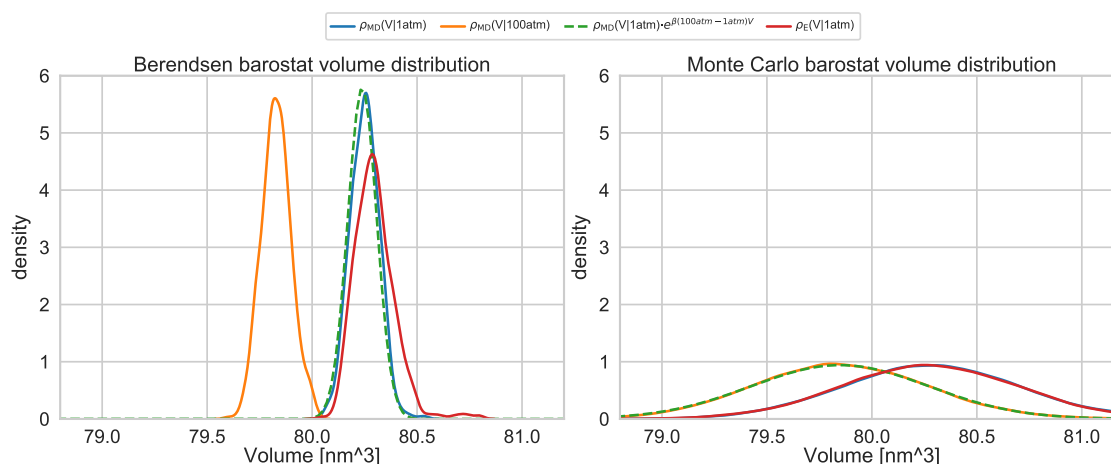


Figure 4. OA-G3 volume distribution, restraint radius distributions, and binding free energy dependency on the binding site definition. Box volume empirical distributions obtained by NPT simulations using the Monte Carlo barostat implemented in OpenMM (right) and the Berendsen barostat implemented in GROMACS (left) at 298 K. The continuous blue ($\rho_{\text{MD}}(V|1\text{atm})$) and orange ($\rho_{\text{MD}}(V|100\text{atm})$) lines represent Gaussian kernel density estimates of volume distributions sampled with simple molecular dynamics at a constant pressure of 1 atm and 100 atm respectively. The green distribution is obtained by reweighting $\rho_{\text{MD}}(V|1\text{atm})$ to 100 atm. The red densities ($\rho_{\text{MD}}(V|1\text{atm})$) represent the volume distribution sampled in the bound state by the enhanced sampling algorithm (i.e., expanded ensemble for the Berendsen barostat and HREX for the Monte Carlo barostat). The expected distribution is predicted correctly only from the volumes sampled using the Monte Carlo barostat, while the Berendsen barostat samples distributions of similar mean but much smaller fluctuations. Moreover, the expanded ensemble algorithm introduce artifacts in the volumes sampled by the Berendsen barostat.

616 where the sign of the RMSE relative efficiency is not statistically significant. In particular, the estimator
 617 based on the Gaussian approximation of the work distribution can be significantly unstable for both the
 618 forward (e.g. CB8-G3) and the reverse (e.g. OA-G3) directions. This may be due to the Gaussian estimator's
 619 linear dependency on the work variance, which makes its free energy estimate sensitive to rare events
 620 that do not affect Jarzynski's estimator. For example, the average free energy profile obtained for OA-G3
 621 with the Gaussian estimator in the reverse direction (i.e. Gaussian-Reverse) displays a "saw-like" pattern
 622 with large and sudden jumps in the average free energy that are due to single rare events with large work
 623 dissipation which substantially increase the variance of the work distribution (SI Figure 10). The work variance
 624 subsequently gradually decreases when more regular events are introduced. Moreover, all unidirectional
 625 estimates for CB8-G3 are significantly biased, and none of them agree with the bidirectional estimates within
 626 statistical uncertainty. In general, this data suggests that collecting nonequilibrium switching trajectories in
 627 both directions is worth the cost of generating samples from the equilibrium distributions at both endpoints
 628 of the alchemical transformations.

629 3.5 The Berendsen barostat introduces artifacts in expanded ensemble calculations

630 Initially, the GROMACS/EE free energy calculations were performed in the NPT ensemble, but these converged
 631 to different binding free energies than the reference OpenMM/HREX calculations performed with YANK. In
 632 order to understand the origin of this discrepancy, we looked into the differences in the protocols adopted by
 633 the two methods that could have affected the asymptotic binding free energies. In particular, we examined
 634 the robustness of the reweighting step used by YANK at the end points to remove the bias introduced by
 635 the harmonic restraint (see also Detailed methods section), the sensitivity of the calculations to the PME
 636 parameters (i.e. FFT grid, error tolerance, and spline order), and the barostat employed.

637 After verifying that the reweighting step and the PME parameters did not impact significantly the free
 638 energies predicted by the two methods (SI Figure 2 and SI Table 6), we investigated the effect of the
 639 barostat on the asymptotic binding free energy. OpenMM used Metropolis-Hastings Monte Carlo molecular
 640 scaling barostat [104, 105] while GROMACS a continuous scaling (or Berendsen) barostat [106]. Because

of implementation issues, only the Berendsen barostat was compatible with both expanded ensemble simulations and bond constraints at the time simulations were run. It is known that the Berendsen barostat does not give the correct volume distribution [107, 108], but in most cases, expectations of variables relatively uncorrelated to the volume fluctuations, such as energy derivatives in alchemical variables, might be expected to be essentially unaffected. We thus re-ran both methods in NVT, first with different and then identical PME parameters. If the NVT calculation is run at the average NPT volume, we expect the NVT and NPT binding free energy predictions to be essentially identical as, in the thermodynamic limit, $dG = dA + d(pV)$, where G and A are the Gibbs (NPT) and Helmholtz (NVT) free energies respectively, and we expect $1 \text{ atm} \cdot \Delta \bar{V}$, where \bar{V} is the change in volume on binding, to be negligible. The box vectors used for the NVT calculations were selected from the OpenMM/HREX NPT trajectories in order to obtain the volume closest to the average NPT volume. The changes introduced by the different PME parameters were not statistically significant (SI Table 6), but we found that the discrepancies between the methods vanished without the barostats. In particular, OpenMM/HREX yielded free energies identical to those obtained at NPT, whereas the expanded ensemble predictions for OA-G3 decreased by 0.6 kcal/mol, suggesting that the Berendsen barostat was responsible for generating artifacts in the simulation.

To obtain further insight, we performed molecular dynamics simulations of OA-G3 at 1 atm and 100 atm in NPT using the GROMACS Berendsen barostat and the OpenMM Monte Carlo barostat. We found that the Berendsen barostat generated volume distributions with much smaller fluctuations and slightly different means than the MC barostat. At 1 atm, the mean of the Berendsen and MC barostat distributions are $80.250 \pm 0.006 \text{ nm}^3$ and $80.286 \pm 0.004 \text{ nm}^3$ respectively (errors here are two times the standard error of the mean). In contrast to the MC barostat, reweighting the distribution generated by the Berendsen barostat at 1 atm with the weight $e^{\beta(100\text{atm}-1\text{atm})V}$ fails to recover the 100 atm distribution (Figure 4), which confirms that the Berendsen barostat did not sample correctly the expected volume fluctuations in the NPT ensemble. Moreover, the volume distribution sampled in the bound state by the Berendsen barostat during the expanded ensemble calculations is quite different from that obtained through simple MD simulations, with thicker right tails and mean $80.298 \pm 0.008 \text{ nm}^3$. The apparent shift to the right is consistent with the volume expansion observed in the neighbor intermediate states during the expanded ensemble calculations (SI Figure 8), which suggests that the artifacts might be introduced by the random walk along states. In principle, we expect the difference in binding free energy due to the different barostats to be approximately $p(\Delta \bar{V}_{\text{MC}} - \Delta \bar{V}_{\text{B}})$, where $\Delta \bar{V}_{\text{MC/B}}$ is the change in volume on binding from according to the MC or Berendsen barostat, as indicated. However, because the mean volume for the Berendsen and MC barostats are different even for the simple MD simulation, it is not completely clear whether a difference in free energy would still be present without the expanded ensemble algorithm. In fact, the mean bound state volume obtained by the Berendsen barostat during the expanded ensemble calculation is closer to the MC mean volume than the one obtained with MD. Further free energy calculations using the Berendsen barostat but independent λ windows might be helpful in clarifying this issue.

3.6 Estimators of the free energy variance based on correlation analysis can underestimate the uncertainty

Since participants also submitted uncertainty estimates for each of the five replicate calculations, we were able to verify how accurately the different uncertainty estimators could reproduce the true standard deviation of the ΔG estimates, here referred to as $\text{std}(\Delta G)$, from a single run. OpenMM/HREX, GROMACS/EE, and SOMD estimated the single-replicate uncertainties from the asymptotic variance estimator of MBAR after decorrelating the potential based on estimates of the integrated autocorrelation time. AMBER/APR instead used blocking analysis to compute the mean and standard error of $dU/d\lambda$ in each window. These statistics were then used to generate 1000 bootstrapped splines, and the uncertainty was determined by computing the standard deviation of the free energies from the thermodynamic integration of the bootstrapped splines. Finally, GROMACS/NS-DS/SB estimated the uncertainties by running an ensemble of 10 independent non-equilibrium switching calculations for each of the 5 replicate calculations and computing their standard deviations. We built $\hat{s}(\Delta G)$, our best estimate of $\text{std}(\Delta G)$, with 95% confidence intervals for each method by computing the standard deviation of the five replicated free energy predictions. Under the assumption of

691 normally-distributed ΔG , $\hat{s}(\Delta G)$ is distributed according to $\hat{s}(\Delta G) \sim \chi_{N-1} \text{std}(\Delta G)/(N-1)$, where $N = 5$ is the
692 number of replicates [109], which makes it trivial to build confidence intervals around $\hat{s}(\Delta G)$.

693 Under this statistical analysis, the single-replicate trajectories of most methods are within the confidence
694 interval of $\hat{s}(\Delta G)$ (SI Figure 9). In particular, the standard deviations of the single GROMACS/NS-DS/SB
695 replicate calculations generally agree within statistical uncertainty to our best estimate. This is probably
696 expected as both are based on independent calculations. The AMBER/APR uncertainty estimates based on
697 bootstrapping also agree well with the replicate-based estimate, especially in the final part of the trajectory.
698 We note, however, that the MBAR standard deviation estimate based on autocorrelation analysis statistically
699 underestimates $\hat{s}(\Delta G)$ in OpenMM/SOMD, and, in general, it shows a marked tendency to be on the lower
700 end of the confidence interval also in OpenMM/HREX and GROMACS/EE. These observations are consistent
701 with those of a prior comparison of the autocorrelation and blocking analysis methods [94]. Similarly, the
702 BAR standard deviation in the NAMD/BAR submission did well for the two octa acids, but the uncertainty
703 was significantly underestimated for the CB8-G3, in which the true standard deviation was on the order of
704 1.2 kcal/mol. Curiously, the MBAR uncertainties are almost identical across the five replicates in all three
705 submissions using them and for all systems. This is in contrast not only to bootstrap- and replicate-based
706 methods but also to the BAR uncertainty estimates submitted by NAMD/BAR, which seem to yield estimates
707 that are more sensitive to differences in the single free energy trajectories.

708 In order to verify if the performance of the MBAR uncertainties was due to an inadequate decorrelation
709 of the samples, we analyzed again the HREX data after raising the interval used for subsampling from
710 approximately 2.8 ps to 5, 10, 20, 50, 100 and 200 ps. In this case, the equilibration time, and thus the
711 number of initial iterations discarded, was determined as two times the statistical inefficiency. As SI Figure 11
712 shows, setting the statistical inefficiency to 5 ps is sufficient for the single-replicate uncertainty to fall within
713 the best estimate confidence interval, and arguably, the agreement becomes slightly better with greater
714 values of statistical inefficiency. However, the single-replicate uncertainties are still almost identical across
715 the five replicates even for the estimates obtained with statistical inefficiency set at 200 ps, in which, due
716 to the limited number of samples, the individual free energy trajectories are quite different and show
717 very different errors. Thus, while the error computed through autocorrelation analysis is within statistical
718 uncertainty of the standard deviation, the estimates seem insensitive to the particular realization of the free
719 energy trajectory.

720 **3.7 The initial bias of HREX is explained by the starting population of the replicas**

721 The initial conformation can bias the free energy in systems with long correlation times
722 In all three host-guest systems, we noticed that the OpenMM/HREX free energy trajectories were significantly
723 biased at the beginning of the calculation. The problem was particularly evident for the CB8-G3 system, for
724 which the performance of methods was generally poorer, and a lot of computational effort was required
725 for the bias to decay in comparison to OA-G3 and OA-G6. *Figure 5* shows that the initial bias of CB8-G3
726 gradually disappears when an increasing amount of data from the initial portion of the calculation is ignored
727 during the analysis. This suggests the initial conditions to be the cause of the bias. This becomes apparent
728 when realizing that the HREX free energy trajectory in *Figure 5* observed after discarding 2000 iterations
729 can be interpreted as from HREX calculations starting from different initial conditions. What is peculiar
730 about this equilibration process is the consistent sign of the observed bias (i.e. $\mathbb{E}[\Delta G_X] - \Delta G_\theta < 0$), which
731 remains negative even after several thousands iterations are removed (1000 iterations corresponding to
732 the equivalent of 131 ns of aggregate simulation from all replicas). The same trend is observed both for
733 OA-G3 and OA-G6, although the correlation times governing the equilibration process appear much smaller
734 in these two cases than with CB8-G3.

735 Initializing all replicas with a bound structure might be the cause of the negative sign of the bias
736 Decomposing the free energy in terms of contributions from complex and solvent legs of the HREX calculation
737 shows that the finite-time bias is entirely attributable to the complex phase (SI Figure 13). As it is common to
738 do with multiple-replica methodologies, all HREX replicas were seeded with the same initial conformation,
739 which, for the complex phase, was obtained by equilibrating the docked structures for 1 ns in the bound state.

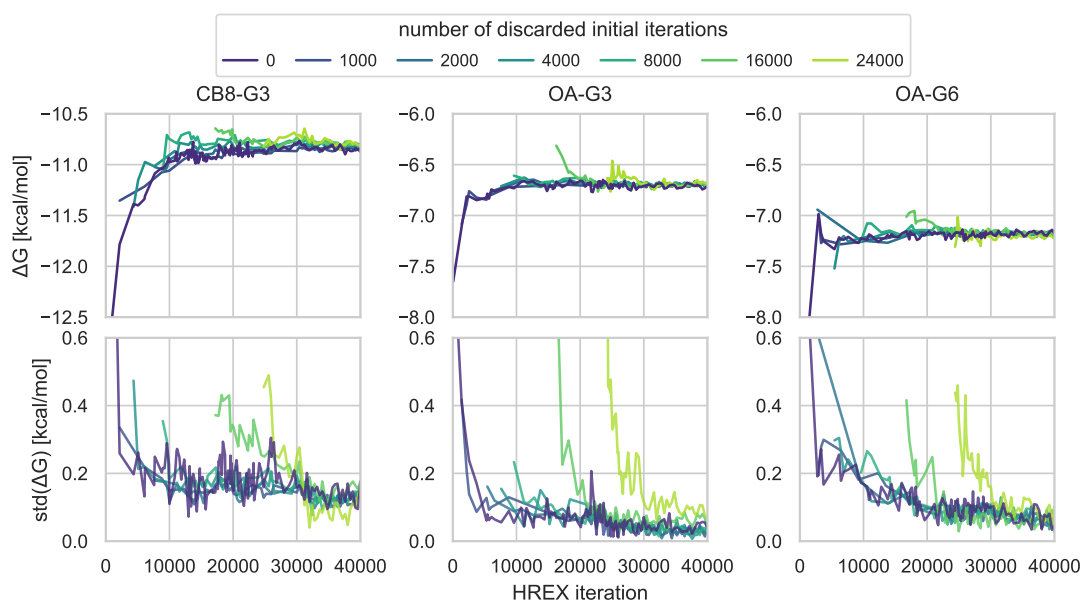


Figure 5. Initiating the HREX calculation from a single conformation introduces significant bias that slowly relaxes as the system reaches equilibrium. Mean (top row) and standard deviation (bottom row) of the five replicate free energy trajectories as a function of the simulation length computed after discarding an increasing number of initial iterations going from 1000 (purple) to 24000 (light green) for the three host-guest systems. The trajectories are plotted starting from the last discarded iteration. The initial bias is consistently negative, and it decays faster in OA-G3/G6 than in CB8-G3, in which correlation times are longer. Ignoring the beginning of the trajectory removes the bias.

740 The so-obtained initial structure is representative of the bound state, and we expect it to decorrelate quickly
741 in the decoupled state thanks to the missing steric barriers and the Monte Carlo rotations and translations
742 performed by YANK. On the other hand, the intermediate states might require a long time to relax the initial
743 conformation, during which the generated samples will be closer to the bound state distribution than if they
744 had been sampled from the intermediate states equilibrium distribution. Under these conditions, the free
745 energy estimator will predict the bound state to have a lower negative free energy. A detailed explanation of
746 this last fact can be found in Appendix 3 in the supporting information.

747 An alternative explanation for the negative sign of the bias relies on the increase in entropy that often
748 accompany the transformation from the bound to the decoupled state. This is usually attributed to the
749 larger phase space available to receptor and ligand and to solvent reorganization [110], and, in this instance,
750 it is confirmed by the entropy/enthalpy decomposition of the predicted free energy (SI Figure 14). The
751 hypothesis relies on the assumption that the larger phase space available in the decoupled state would
752 require thorough sampling to be estimated correctly, which would be impossible at the beginning of the
753 calculation when the estimate would be computed from a small number of correlated samples. As a result,
754 the difference in entropy between the end states would initially be underestimated, and the binding free
755 energy would become more positive as the number of samples enables a more precise prediction. However,
756 this hypothesis seems unlikely, at least in this case, as it does not explain why ignoring the initial part of the
757 calculation would result in an unbiased estimate since the beginning of the free energy trajectory would still
758 be based on an equivalently small number of samples. The large fluctuations of the estimated entropy and
759 potential energy trajectories, which are in the range of 10-20 kcal/mol (SI Figure 14) against a bias of less
760 than 2 kcal/mol, hinder the direct verification of the two hypotheses, but further investigation of the cause
761 and sistematicity of the negative bias across different receptor-ligand systems is currently ongoing.

762 Relevance for other methods

763 While, for reason of data availability, we focused on HREX here, it should be noted that, in principle, this is
764 not a problem confined to the HREX methodology, and most free energy trajectories generated by alchemical

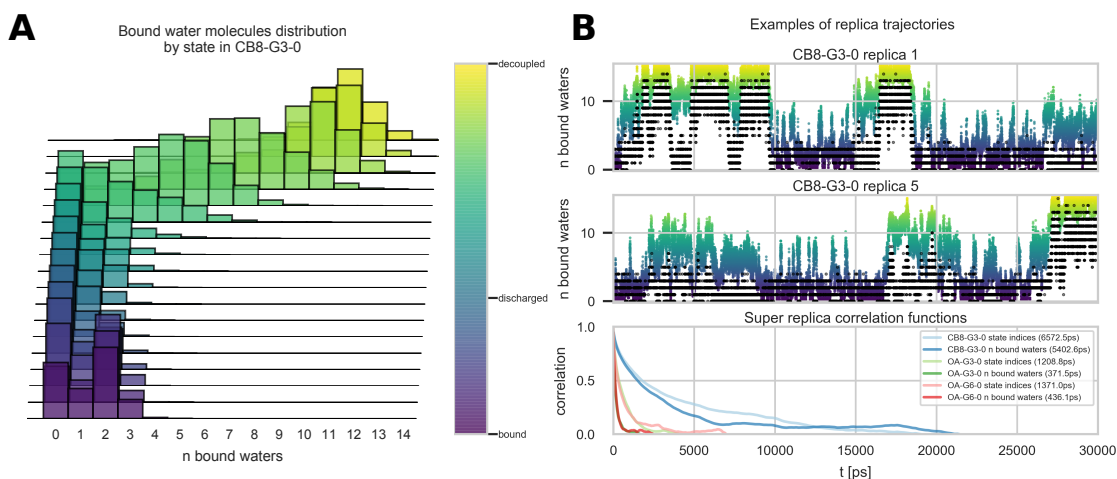


Figure 6. Bound water molecules induce metastability in HREX replicas with CB8-G3. (A) Histograms of the number of bound water by thermodynamic state. The color maps the progression of the alchemical protocol from the bound state (purple) to the discharged state (blue), where all the charges are turned off but Lennard-Jones interactions are still active, and decoupled state (yellow). The number of bound waters has a peaked distribution around 0-2 for most of the alchemical protocol, and it rapidly shifts to the right in the near-decoupled state. (B) Superposition of the trajectories of the number of bound waters and the state index for replica 1 and 5 of the OpenMM/HREX calculation for CB8-G3-0 (top) and autocorrelation function computed from the time series of the number of bound waters (dark colors) and replica state indices (light colors) for CB8-G3-0 (blue), OA-G3-0 (green), and OA-G6-0 (red) (bottom). Each autocorrelation function was computed as the average of the correlation functions estimated for each replica trajectory [39, 111]. Replicas remain stuck in the near-decoupled states for several nanoseconds. CB8-G3 exhibits much longer correlation times for both time series than the two OA systems.

765 methods show an initial upward trend in all three host-guest systems that may be due to one of these
766 two explanations. In fact, the bias of HREX in CB8-G3 seems to decay faster than other multiple-replica
767 double decoupling methods (i.e., NAMD/BAR and OpenMM/SOMD), whose free energy estimates are still
768 significantly more negative when compared to more converged estimates (e.g., APR, HREX, NS-DS/SB) at
769 the same computational cost (Figure 2). This is consistent with our hypothesis as the enhanced sampling
770 strategy should help reducing correlation times of the intermediate states as well. Indeed, while we could
771 not identify a specific physical collective variable responsible for the slow decorrelation of the intermediate
772 states, the correlation time of the replica state index is consistent with the bias decay time in CB8-G3 and
773 OA-G3/G6 (Figure 6).

774 The data suggest that cheap methods for the determination of sensible initial conformations for the
775 intermediate states may improve considerably the efficiency of HREX in systems with long correlation times.
776 Moreover, a better trade-off between bias and variance in the final estimate could be achieved with better
777 strategies for automatic equilibration detection or by reducing the number of intermediate states (69 for the
778 complex and 62 for the solvent in the CB8-G3 HREX calculations), which directly impact the total number of
779 energy evaluations spent equilibrating the replicas.

780 3.8 Water binding/unbinding in CB8-G3 might contribute to long correlation times in 781 HREX

782 In order to get insights into the origin of the large uncertainties generally obtained by the double decoupling
783 submissions for the CB8-G3 system, we analyzed the correlation times of various collective variables (CV)
784 in the complex phase of the OpenMM/HREX calculations. Figure 6 shows that the number of waters in
785 the binding site of CB8-G3 is metastable and correlate with the state index of the replicas (where each
786 replica of the Hamiltonian replica exchange calculation can explore multiple states). The number of bound
787 waters was computed by counting the water molecules with at least one atom within the convex hull of
788 the heavy atoms of CB8. The metastability along replica trajectories depicted in Figure 6B is connected
789 to a rapid shift towards greater numbers of the distribution of bound waters near the decoupled state

790 (**Figure 6A**). This contrasts with the discharging step, where the only evident change is a change in the mode
791 of the bound water histogram from 2 to 0. The shift in mode is consistent with the observed distribution of
792 restrained distance between host and guest (SI Figure 2), which suggests that the guest tends to crawl into
793 the hydrophobic binding site in the discharged state to compensate for the loss of the polar interactions with
794 water. Histograms of the number of bound waters for OA-G3 and OA-G6 (SI Figure 16) show similar features
795 to that of CB8-G3, but the mean number of bound waters in the decoupled state is smaller (i.e. 4.84 water
796 molecules) due to the smaller volume of the octa-acid binding site. Moreover, the statistical inefficiency
797 computed from the correlation function of the state index, which was previously found to correlate well with
798 the uncertainty of free energy estimates in Hamiltonian replica exchange calculations [39], is about five
799 times smaller for OA-G3/G6 (1208.8 ps and 1371.0 ps) than for CB-G3 (6572.3 ps). This is consistent with the
800 slower convergence generally observed for the latter set of calculations.

801 While these results prove only the existence of correlation between the metastabilities in the number
802 of bound waters and the state indices along a replica trajectory in the CB8-G3 calculations, it is plausible
803 to hypothesize that water molecules displaced by the quinine when the Lennard-Jones interactions are
804 re-coupled, alongside eventual steric clashes with the host binding site, might contribute significantly to
805 hindering the replica exchange step with obvious negative effects on the ability of the HREX algorithm to
806 enhance sampling. This is consistent with the faster replica exchange mixing observed for OA-G3/G6 as
807 coupling the guest would have to displace a smaller number of bound waters than CB8-G3 due to the smaller
808 volume of the guests. No other CV we analyzed had statistical inefficiencies on the same order of magnitude
809 as those observed for the bias decay time shown in **Figure 5**. In particular, both the host-guest distance
810 restrained by the harmonic potential and the distance between the alchemically-decoupled counterion and
811 the guest seem to decorrelate quickly along replica trajectories, with estimated statistical inefficiencies never
812 exceeding 50 ps. Possibly, an increased number of intermediate states close to the decoupled state might
813 enhance the replica exchange acceptance rates for CB8-G3 and reduce the statistical inefficiency of the state
814 index.

815 **3.9 Methods generally overestimated the host-guest binding free energies with respect** 816 **to experimental measurements**

817 Accuracy with respect to experiments was not the focus of this study, but the input files for the challenge
818 were created using a quite typical setup, and it is thus interesting to compare the converged predictions to
819 the corresponding experimental data collected for the accuracy host-guest challenge [26, 112, 113]. The ITC
820 measurements yielded binding free energies of -6.45 ± 0.06 kcal/mol for CB8-G3, -5.18 ± 0.02 kcal/mol for
821 OA-G3, and -4.97 ± 0.02 kcal/mol for OA-G6. In comparison, the well-converged computational results were more
822 negative on average by -4.4 , -1.2 , and -2.1 kcal/mol respectively, in line with what was observed for other
823 methods employing the GAFF force field in the SAMPL6 host-guest accuracy challenge [26]. It should be
824 noted that the ionic strengths of SAMPLing systems (i.e., 150 mM for CB8-G3 and 60 mM for OA-G3/G6)
825 were slightly higher than in experimental conditions (estimated to be 57.8 mM for CB8-G3 and 41.25 mM
826 for OA-G3/G6) used for the host-guest binding challenge, and previous evidence revealed the host-guest
827 binding free energies to be sensitive to concentration and composition of the ions. In a recent SOMD
828 calculations performed for the SAMPL6 accuracy challenge, removing the ions modeling ionic strength of the
829 experimental buffer (i.e. going from 150 mM for CB8-G3 and 60 mM OA-G3/G6 to 0 mM) caused the ΔG
830 prediction to shift by -4.87 ± 2.42 , 1.37 ± 0.50 , and 1.48 ± 0.48 for CB8-G3, OA-G3, and OA-G6 respectively
831 (computed as the average of three runs \pm standard error of the mean) [76]. In particular, the estimated
832 binding free energy for OA-G3 obtained without buffer ions agreed with the experimental measurement
833 within uncertainty. It is unlikely for the ion concentrations to be the sole responsible for the overestimated
834 binding affinities. The sign of the shift for CB8-G3 described above is not consistent with the hypothesis,
835 and a negative mean error was very consistent across GAFF submissions employing different buffer models.
836 Nevertheless, the order of magnitude of these shifts suggests that ionic strengths cannot be neglected.

837 **4 Discussion**

838 **4.1 Disagreements between methodologies impact force field development and** 839 **evaluation**

840 In many cases, methods obtained statistically indistinguishable predictions with very high precision. The
841 agreement between methodologies is quite good for OA-G6, where essentially all estimates are within
842 0.4 kcal/mol. On the other hand, despite the focus of the study on reproducibility, some of the methods
843 yielded predictions that significantly deviated from each other by about 0.3 to 1.0 kcal/mol. This directly
844 raises a problem with force field evaluation and development since it implies that the accuracy afforded
845 by a given set of forcefield parameters (and thus the value of the loss function used for their training) can,
846 in practice, be affected significantly by the software package, methodological choices, and/or details of
847 simulation that are considered to have negligible impact on the predictions (e.g., switched vs truncated
848 cutoff, treatment of long-range interactions, ion concentrations). Trivially, this also implies that we should
849 not expect a force field to maintain its accuracy when using simulation settings that differ from those used
850 during fitting.

851 Similar observations were made in previous work in different contexts. In a reproducibility study involving
852 four different implementations of relative hydration free energy calculations, the authors found in many
853 cases statistically significant $\Delta\Delta G$ differences on the order of 0.2 kcal/mol [30]. Systematic differences of the
854 same order of magnitude were detected in a recent study comparing Monte Carlo and Molecular Dynamics
855 sampling for binding free energy calculations [27], although, in this case, differences in water models and
856 periodic boundary conditions might confound the analysis.

857 **4.2 Bias is critical when comparing the efficiency of different methodologies**

858 The results show that quantifying not only the variance but also the bias of a binding free energy method is
859 important to draw a complete picture of the efficiency of a method. The bias of the free energy predictions
860 varied substantially depending on the method and the system, and for calculations that are short with
861 respect to the correlation times, the bias can be greater or have the same order of magnitude of the variance.
862 For example, in CB8-G3, NS-DS/SB-long obtained a greater RMSE efficiency than HREX in spite of the similar
863 variance because the bias of OpenMM/HREX for CB8-G3 remained non-negligible for a substantial portion of
864 the calculation. This suggests that looking at the variance of the free energy estimate alone is insufficient to
865 capture the efficiency of a method, and the RMSE relative to the asymptotic binding free energy prediction
866 should be favored as the main statistic used in studies focusing on exploring and testing methodological
867 improvements.

868 Estimating the RMSE and bias is a more complicated problem than estimating the variance as it requires
869 the value of asymptotic free energy given by the model and thus to ascertain that the calculation has
870 converged. Visual inspection of the free energy trajectory is useful, but it can be misleading. Besides the
871 presence of unexplored relevant areas of configurational space, the noise in the trajectory can hide very
872 slow decays (see YANK calculation in CB8-G3). More recommendations about how to detect convergence
873 issues can be found in [114, 115].

874 On the other hand, a focus on quantifying the efficiency of free energy calculations in terms of RMSE could
875 increase the attention paid to convergence issues as well as incentivize the creation of reference datasets
876 that could provide asymptotic free energies associated to specific input files without always requiring long
877 and expensive calculations. The latter would particularly benefit the field when the efficiency of a method
878 would need to be evaluated only for very short protocols (e.g. overnight predictions). This is, however,
879 conditional on identifying the source of the discrepancies between the predictions of different methods and
880 an asymptotic value can be agreed upon in the first place.

881 **4.3 Multiple replicates are one route to avoiding underestimating the uncertainty**

882 MBAR uncertainties and bootstrap uncertainties built with the blocking method were in most cases able to
883 estimate the standard deviation of the free energy prediction within confidence interval. Nevertheless, when
884 sampling is governed by rare events and systematically misses relevant areas of conformational space, data

885 from a single trajectory simply cannot contain sufficient information to estimate the uncertainty accurately.
886 An example is given by the CB8-G3 calculations performed by OpenMM/SOMD and NAMD/BAR, for which the
887 uncertainty estimates were underestimated by more than 1 kcal/mol. In these cases, replicate calculations
888 starting from independent conformations can offer a solution to or compensate for the problem. Relaxed
889 docked conformations can be a viable method to generate the independent conformations, although this
890 is not, in general, an easy task and multiple short replicates starting from the same or very similar initial
891 conformations can still cause the uncertainty to be underestimated. Moreover, given a limited amount
892 of computational resources, the number of replicate calculations should not be large enough to prevent
893 sampling of all the relevant time scales, which are strongly system-dependent.

894 In addition to a more accurate estimate of the free energy estimate, it has been argued that predictions
895 computed from an ensemble of independent calculations lead to more robust estimates [32, 116]. In
896 agreement with these results, the simple average of the five independent free energies is surprisingly robust
897 even when the single-replicate predictions do not agree quite well (SI Figures 9,11).

898 **4.4 Shortcomings of the analysis and lesson learned for future studies**

899 The bias estimation strategy favors short and unconverged calculations

900 Originally, the calculations run by the organizers (i.e., OpenMM/HREX and GROMACS/EE) were meant to
901 provide a reference estimate of the asymptotic free energy of the model that we could use to detect and
902 estimate systematic biases. However, because of the differences in setups and treatment of long-range
903 interactions adopted in the different submissions, this type of analysis was not possible. Instead, we
904 estimated the asymptotic free energy for each methodology as the average binding free energy of the 5
905 replicates after 100% of the computational cost. As a consequence, the bias is generally underestimated,
906 and long calculations and converged results are thus generally penalized in the calculation of the efficiency
907 statistic. Some of these differences could be minimized by picking settings to which most software packages
908 and methods will be able to adhere. For example, providing systems solvated in both cubic and elongated
909 orthorhombic boxes, and running reference calculations for both of them, could lower the barrier for PMF
910 calculations to enter the challenge without re-solvating the reference files. Moreover, using a truncated cutoff
911 instead of a switched cutoff could help as AMBER does not support switched cutoffs and different simulation
912 packages could use slightly different switching functions. Also, providing template input configuration files
913 for common simulation packages that encapsulate other settings such as PME parameters could reduce the
914 risk of running several methods with different settings.

915 The number of force evaluations can miss important information about the computational cost
916 In this work, we have focused the analysis on the number of energy/force evaluations as a measure of
917 the methods' computational cost. In general, this is a very practical and fair measure of the cost of a
918 method. For example, unlike wall-clock or CPU time, it does not depend on hardware and the particular
919 implementation, which is compatible with the objective of this challenge in detecting fundamental differences
920 in efficiency between algorithms. Thus, even though implementation details might affect wall-clock/GPU
921 time dramatically, methods with a comparable number of energy/force evaluations might eventually be able
922 to be put on equal footing given enough developer time if it seemed warranted. Moreover, this measure
923 treats both molecular dynamics and Monte Carlo strategies equally, which would not be possible if the cost
924 was measured, for example, in terms of simulation time (e.g., nanoseconds of simulation).

925 However, the number of force/energy evaluations can miss important details. It is insensitive to the
926 system size, and it assumes that the computational cost of all other components of the calculation is
927 negligible. Furthermore, while some sampling schemes require multiple evaluations of the Hamiltonian,
928 often it is not necessary to compute it in its entirety. For example, in multiple time scale MD and Monte
929 Carlo moves involving a reduced number of degrees of freedom, one only needs to compute a subset of
930 pairwise interactions. HREX requires the evaluation of multiple Hamiltonian at the same coordinates, but
931 only the parts of the Hamiltonian that change between intermediate state needs to be evaluated multiple
932 times. When the algorithms and setups differ, this may become important to take into account. For example,
933 double decoupling methods assigned the same computational cost to each time step of the complex and

934 solvent stages of the calculation, while REVO, APR, and NS-DS/SB ran only in one stage using a box of the
935 same or greater size of the complex so that one force evaluation for the latter methods on average is
936 practically more expensive than a force evaluation for double decoupling.

937 In future challenges, it might be useful to collect another simple but more precise measure of the
938 computational cost of a method based on a scaled version of the number of energy/force evaluations, with
939 the scaling factor depending on the number of particles that enters the evaluation. Moreover, instead
940 of requesting exactly 100 free energy estimates for each replicate, requesting free energy estimates that
941 are roughly equally spaced by a predetermined number of force/energy evaluations could make it simpler
942 to perform direct comparisons between all methods without requiring the comparison to a reference
943 calculation.

944 A larger and more varied test set is necessary to obtain a more comprehensive picture of the
945 methods' efficiency

946 This first round of the challenge was created as a component of the SAMPL6 host-guest challenge, and we
947 created a minimal test set including both fragment-like and drug-like compounds. We believe this was a
948 beneficial decision. Fragment-like guests that converged relatively quickly such as OA-G3/G6 proved very
949 useful to debug systematic differences between methods while most of the methods problems or strengths
950 were unveiled from the calculations targeting CB8-G3, which has a greater size and generally proved to be
951 more challenging for free energy methods than the two octa-acid guests.

952 Expanding the test set to include one trivial system and a few more challenging systems could increase
953 the potential for learning and provide a more complete picture of the problems to address and the domain
954 of applicability of the different methods, especially as different approaches may have different strengths and
955 weaknesses. For example, HREX and EE could be less effective at improving convergence for systems with
956 a single dominant binding mode. On the other hand, systems with a buried binding pocket that remains
957 dry in both the holo and apo states could be less problematic for HREX and EE, which are challenged by
958 wetting/dewetting processes that occur at the "almost decoupled" state. At the same time, physical-pathway
959 methods such as APR and REVO might be less effective for receptor-ligand systems with buried binding
960 pockets, as an efficient unbinding path could require large reorganization of the receptor that might be
961 difficult to determine or sample.

962 For systems that are easier to converge, it might also be possible to increase the number of replicates
963 from five. The increased statistical power could be particularly helpful to resolve differences between
964 methods in efficiency, in estimated binding free energy predictions, and for the analysis of the uncertainty
965 estimates (e.g. blocking, bootstrap, and correlation analysis) since the standard deviation of the binding free
966 energy estimated from five replicates have large variance, which makes it hard to draw statistically significant
967 conclusions. For bigger systems, this may not be practical, but the number of replicates does not necessarily
968 have to be the same for all the tested systems.

969 Finally, we point out that the selection of systems for such convergence studies is not limited by the lack
970 of experimental data or a chemical synthesis route, and one is free to craft an optimal test system.

971 **4.5 Parallelization considerations**

972 The analysis above does not account for the differences in the intrinsic levels of parallelization of the different
973 methods, but almost all methods can be completely or almost trivially parallelized over up to 40 parallel
974 processing units with the given protocols. APR, NAMB/BAR, and SOMD protocols use respectively 60, 64, and
975 40 windows, the last two numbers to be divided equally between complex and solvent stages. Each HREX
976 calculation ran more than 100 MC/MD parallel simulations, although the exchange step provides a bottleneck
977 for the simulation. Similarly, the protocol used for the REVO methodology employs 48 independent walkers
978 that can be run in parallel throughout the calculation, with a bottleneck occurring at the cloning/merging
979 stage of the adaptive algorithm. NS-DS/SB protocol used 10 independent equilibrium simulations for each
980 end state (i.e. bound and unbound states) that generate frames used to spawn nonequilibrium switching
981 trajectories in both directions. New NS trajectories can be started as soon as new equilibrium samples are
982 generated. Thus, because the nonequilibrium trajectory duration in this protocol is greater than the interval

983 between two equilibrium frame, the calculation can in principle have at least 40 independent simulations
984 running in parallel. The EE protocol submitted for this work is an exception as it does not use a parallelization
985 scheme, although maintaining and coordinating multiple independent expanded ensemble chains is in
986 principle possible [117].

987 Nevertheless, all calculations can also be trivially parallelized over the molecules in the set and over
988 eventual independent replicate calculations. Under perfect parallelization, or in the presence of negligible
989 bottlenecks, the relative efficiency is insensitive to the number of parallel processing units so we expect
990 the analysis in this work can be informative also in many common scenarios involving parallel computing
991 systems. However, these results should be careful re-interpreted in the presence of massively parallel
992 computational systems, in which the number of processing units does not provide a fundamental bottleneck.
993 For example, a large number of GPUs could be exploited better with protocols simulating many intermediate
994 states that can be simulated in parallel, such as those used by HREX and APR.

995 **4.6 Relevance and future plans for relative free energy calculations**

996 Unfortunately, we did not receive any relative free energy submission for this round of the challenge.
997 However, the data reported here has implications for relative calculations as well. Given that enhanced
998 sampling strategies based on Hamiltonian exchange had little or no impact on efficiency for the octa-acid
999 systems, we expect a relative calculation to be significantly more efficient than two absolute calculations in
1000 computing a $\Delta\Delta G$ value for the simple OA-G3 to OA-G6 transformation that we set up. For the same reason,
1001 we would expect enhanced and non-enhanced relative methods to perform similarly for the OA-G3 to OA-G6
1002 transformation. On the contrary, a relative transformation involving a system with long correlation times such
1003 as CB8-G3 might benefit more from enhanced sampling strategies and be less sensitive to the initial bound
1004 conformation. Finally, while cancellation of error might help, we expect to observe discrepancies between
1005 different packages and/or methods also for relative calculations as, with the exception of OpenMM/HREX
1006 and AMBER/APR, the $\Delta\Delta G$ between methods does not appear to be systematic.

1007 In future rounds of the challenge, we are interested in probing the boundaries of applicability of this
1008 technology, particularly in the presence of ligands or alchemical transformations requiring exploration of
1009 multiple, kinetically-separated binding modes. For these cases, state-of-the-art methods in both absolute
1010 and relative calculations often rely on scaling selected Coulomb, Lennard-Jones, and/or torsional terms of
1011 the Hamiltonian to lower the energetic barriers between relevant conformations [35, 118] Typically, the
1012 optimal choice for the range of scaling factors and the subset of the systems to enhance is very system-
1013 dependent, not known *a priori*, and essentially determined by a trade-off between shortening mixing times
1014 and simulating extra intermediate states sharing poor overlap with the end states of the transformation.
1015 In this sense, absolute methods such as HREX and EE bring this trade-off to an extreme by turning off
1016 completely receptor-ligand electrostatics and sterics interactions. This enables dramatic changes in binding
1017 pose, such as the upside-down flip of CB8-G3, at the cost of introducing states with poor overlap with the
1018 end states, although without usually modifying torsions or receptor atoms that would reduce the overlap
1019 even further. Again, careful selection of the receptor-ligand systems will be fundamental to determine under
1020 which conditions protocols favoring sampling or statistical efficiency would result in faster convergence.

1021 **5 Conclusions**

1022 We have presented the results of the first round of the SAMPLing challenge from the SAMPL challenge series.
1023 The design and execution of the challenge made apparent the need for a measure of efficiency for free
1024 energy calculations capable of capturing both bias and uncertainty of the finite-length free energy estimates
1025 and summarizing the performance of a method over a range of computational costs. The analysis framework
1026 and efficiency statistics we introduced in this work allow formulation and evaluation of hypotheses regarding
1027 the efficiency of free energy methods that can be verified meaningfully with the standard tools of statistical
1028 inference. We applied this framework to seven free energy methodologies and compared their efficiency
1029 and their level of agreement on a set of three host-guest systems parametrized by the same force field. The
1030 analysis highlighted significant and system-dependent differences in the methods' convergence properties
1031 that depend on both the sampling strategies and the free energy estimator used. Overall, the study shows

1032 that PMF and alchemical absolute binding free energy calculations can converge within reasonable computing
1033 time for this type of system.

1034 Surprisingly, we observed significant differences in the converged free energies for the different methods
1035 ranging from 0.3 to 1.0 kcal/mol. These discrepancies are small enough that they would not have aroused
1036 suspicion without the comparison of multiple independent methods, which stresses the utility and efficacy
1037 of this type of study in detecting methodological problems. While we were able to isolate the origins of some
1038 of these discrepancies, further work will be required to track down the causes of remaining discrepancies,
1039 which might be attributable to small differences in the model (e.g. treatment of long-range interactions,
1040 ionic strength), sampling issues of some of the methods, software package, or any combination of the above.
1041 Notably, the discrepancies between methods are roughly half the size of the current reported inaccuracies of
1042 leading free energy methods compared to experiment (roughly 1 kcal/mol). Eliminating these discrepancies
1043 would therefore be very useful for the field to make further progress.

1044 Although we decided to accept non-blinded submissions to increase the value of the study, future rounds
1045 of the challenge should ideally be limited to blind predictions, in line with the other challenges within the
1046 SAMPL series. The lessons learned while organizing this first round of the challenge will be useful to address
1047 the problems identified during the analysis. In particular, we hope to adopt a slightly different measure
1048 of computational cost based on the number of force/energy evaluations that also takes into account the
1049 system size, and increase the size and variety of the test set. Although an aspirational goal, running on
1050 the same dedicated hardware would allow a meaningful comparison of the performance of the different
1051 methods also in terms of CPU/GPU time, and analyze more closely the speedups obtained with parallelization.
1052 Workflow-ized tools (e.g., Orion workflows, BioSimSpace workflows, HTBAC) could be helpful in pursuing this
1053 direction.

1054 **6 Detailed methods**

1055 **6.1 Preparation of coordinates and parameters files**

1056 The protonation states of host and guest molecules were determined by Epik 4.0013 [119, 120] from the
1057 Schrödinger Suite 2017-2 at pH 7.4 for CB8-G3 and pH 11.7 for OA-G3 and OA-G6. These values correspond
1058 to the pH of the buffer adopted for the experimental measurements performed for the SAMPL6 host-guest
1059 binding affinity challenge. For each host-guest system, 5 docked complexes were generated with rigid
1060 docking using FRED [66, 67] in the OpenEye Toolkit 2017.6.1. Binding poses with a root mean square
1061 deviation less than 0.5 Å with respect to any of the previously generated binding poses were discarded. Hosts
1062 and guests were parameterized with GAFF v1.8 [70] and antechamber [121]. AM1-BCC [68, 69] charges were
1063 generated using OpenEye's QUACPAC toolkit through OpenMolTools 0.8.1. The systems were solvated in a
1064 12 Å buffer of TIP3P [71] water molecules using tleap in AmberTools16 [122] shipped with ambermini 16.16.0.
1065 In order to make relative free energy calculations between OA-G3 and OA-G6 possible, ParmEd 2.7.3 was
1066 used to remove some of the molecules from the OA systems and reduce the solvation box to the same
1067 number of waters. This step was not performed for the CB8-G3 system, and the 5 replicate calculations
1068 were simulated in boxes containing a different number of waters. The systems' net charge was neutralized
1069 with Na⁺ and Cl⁻ ions using Joung-Cheatham parameters [123]. More Na⁺ and Cl⁻ ions were added to reach
1070 the ionic strength of 60 mM for OA-G3/G6 systems and 150 mM for CB8. Note that this ionic strength is likely
1071 to be different from the one used for the experimental measurements, which was estimated to be 41 mM
1072 and 58 mM respectively. Systems were minimized with the L-BFGS optimization algorithm and equilibrated
1073 by running 1 ns of Langevin dynamics (BAOAB splitting [22], 1 fs time step) at 298.15 K with a Monte Carlo
1074 barostat set at 1 atm using OpenMM 7.1.1 [75] and OpenMMTools [124]. Particle Mesh Ewald (PME) was
1075 used for long-range electrostatic interactions with a cutoff of 10 Å. Lennard-Jones interactions used the same
1076 10 Å cutoff and a switching function with a switching distance of 9 Å. After the equilibration, the systems
1077 were serialized into the OpenMM XML format. The rst7 file was generated during the equilibration using the
1078 RestartReporter object in the parmed.openmm module (ParmEd 2.7.3). The AMBER prmtop and rst7 files
1079 were then converted to PDB format by MDTraj 1.9.1 [125]. The files were converted to GROMACS, CHARMM,
1080 LAMMPS, and DESMOND using InterMol [29] (Git hash f691465, May 24, 2017) and ParmEd (Git hash 0bab490,

1081 Dec 11, 2017).

1082 **6.2 Free energy methodologies**

1083 AMBER/APR

1084 We used the attach-pull-release (APR) [93, 94] method to calculate absolute binding free energies of each
1085 host-guest complex. We used 14 "attach" umbrella sampling windows, during which time host-guest complex
1086 restraints are gradually applied, and 46 "pull" umbrella sampling windows to separate the host and guest. A
1087 final, analytic "release" phase was applied to adjust the effective guest concentration to standard conditions
1088 (1 M). Since CB8 has two symmetrically equivalent openings, and the APR method only pulls the guest out of
1089 one opening, we have added an additional $-RT \ln(2) = -0.41$ kcal/mol to the calculated binding free energy
1090 to adjust for this additional equivalent entropic state.

1091 The restraints were setup using our in-development Python package: pAPRika 0.0.3 (commit hash
1092 e69f053). Six restraints (1 distance, 2 angles, and 3 dihedrals) were used to restrain the translational and
1093 orientational degrees of freedom of the host relative to three positionally restrained dummy anchor atoms.
1094 These restraints, which were constant throughout all APR windows, did not perturb the internal degrees of
1095 freedom of the host. The distance force constant was set to 5.0 kcal/mol-Å² and the angle force constant
1096 to 100.0 kcal/mol-rad². Three additional restraints were added, during the attach phase of APR, between
1097 the dummy atoms and two guest atoms in order to orient the guest relative to the host and then separate
1098 the two molecules by 18 Å, which was sufficient for reaching a plateau in the potential of mean force. The
1099 distance and angle force constants for these restraints were the same as before.

1100 All equilibration and production simulations were carried out with the GPU-capable pmemd.cuda MD
1101 engine in the AMBER 18 package [72]. The OA systems were re-solvated with 3000 waters and the CB8
1102 systems were re-solvated with 2500 waters in a orthorhombic box elongated in the pulling direction to
1103 enable distances between the host and guest necessary to carry out the potential of mean force calculation.
1104 Force field parameters and charges of the host-guest systems were not altered in the operation. Equilibration
1105 consisted of 500 steps of energy minimization and enough NPT simulation such that 1 ns could be completed
1106 without the simulation box dimensions changing beyond AMBER limits (up to 10 ns total). All simulations
1107 used a time step of 2 fs, with a Langevin thermostat and a Monte Carlo barostat. The nonbonded cutoff was
1108 set to 9.0 Å, and the default AMBER PME parameters were employed.

1109 For the OA-G3 simulations, we performed 10 ns of sampling per window. For the OA-G6 simulations, we
1110 performed 15 ns of sampling per window. For the CB8-G3 simulations, we performed 70 ns of sampling
1111 per window. In all cases, we used thermodynamic integration to compute the binding free energies. To
1112 compute the uncertainties, we used blocking analysis to calculate the mean and standard error of $dU/d\lambda$
1113 in each window, where U is the potential energy and λ is the reaction coordinate. We then created 1000
1114 bootstrapped splines through points sampled off the distribution determined by the $dU/d\lambda$ mean and
1115 standard error of the mean for each window, used trapezoidal integration for the total free energy for each
1116 spline, and computed the mean and standard deviation of the free energies from the bootstrap samples.

1117 GROMACS/NS-DS/SB and GROMACS/NS-DS/SB-long

1118 The estimates were obtained with alchemical nonequilibrium free energy calculations using GROMACS
1119 2018.3 [73] as described in [90]. Briefly, both legs of the thermodynamic cycle were carried out in the same
1120 box: i.e. one guest molecule was decoupled from the solvent while another copy was coupled while in the
1121 host binding pocket. The two guest molecules were placed 2.5 nm apart and restrained with a single position
1122 restraint on one of their heavy atoms. For the guest molecule bound to the host, a set of restraints as
1123 described by Boresch [91] (1 distance, 2 angles, 3 dihedrals) was applied. A force constants of 10 kcal/mol-Å²
1124 was applied to the distance, and constants of 10 kcal/mol-rad² were applied to the angles.

1125 First, both end-states (A: bound guest coupled and unrestrained, unbound guest decoupled; B: bound
1126 guest decoupled and restrained, unbound guest coupled) were simulated using 10 simulations of 20 ns each
1127 (20.2 ns for CB8), for a total of 400 ns of equilibrium sampling (404 ns for CB8). Each of these 20 simulation
1128 boxes had been previously built from the input files provided by the organizer by re-solvating the host-guest
1129 systems and randomly placing ions in the box at a concentration of 0.1 M, followed by minimization with

1130 10000 steps of steepest descent. The re-solvation was a necessary step to enable sufficient distance between
1131 the host and guest in the unbound state and did not alter the force field parameters of hosts and guests.
1132 However, differently from the challenge input files, Cl⁻ and Na⁺ ions were added to the simulation to reach a
1133 100 mM concentration.

1134 For the OA systems, 50 frames were extracted from each of the equilibrium simulations at an interval
1135 of 400 ps. Thus, in total 500 frames were extracted from the equilibrium simulations of each of the two
1136 end-states. For the CB8 systems, 100 frames were extracted from each of the equilibrium simulations every
1137 200 ps, for a total of 1000 frames. The extracted snapshots were used to spawn rapid nonequilibrium
1138 alchemical transitions between the end-states. In the nonequilibrium trajectories, the Hamiltonian between
1139 the two end states was constructed by linear interpolation.

1140 The alchemical transitions were performed in both directions (A->B and B->A) in 500 ps per simulation
1141 for the OA systems, and in 1000 ps for the CB8 systems. A second submission identified by GROMACS/NS-
1142 DS/SB-long used a 2000 ps nonequilibrium trajectory instead and only for CB8-G3. For the unbound guest,
1143 charges were annihilated (i.e. intra-molecular electrostatics was turned off) and Lennard-Jones interactions
1144 were decoupled (i.e. intra-molecular sterics was left untouched) at the same time, using a soft-core potential
1145 for both. The same protocol was used for the bound guest except that also the Boresch restraints were
1146 switched on/off during the nonequilibrium transitions by linearly scaling the force constants. The two
1147 positional restraints attached to the two copies of the guest were left activated throughout the calculation.
1148 All simulations used Langevin dynamics with a 2 fs time step with constrained hydrogen bonds. Periodic
1149 boundary conditions and Particle Mesh Ewald were employed with a cutoff of 10 Å, interpolation order of
1150 5, and tolerance of 10⁻⁴. A cutoff of 10 Å with a switching function between 9 Å and 10 Å was used for the
1151 Lennard-Jones interactions. An analytical dispersion correction for energy and pressure was also used to
1152 account for the dispersion energy. The Langevin thermostat was set at 298.15 K and a Parrinello-Rahman
1153 barostat [126] was employed to maintain the pressure at 1 atm.

1154 The binding free energy was estimated with pmx [127] from the set of nonequilibrium work with the
1155 BAR [128, 129] estimator after pooling all the data from the ten independent calculations. Uncertainties
1156 were instead estimated by computing the standard error of the ten individual BAR estimates.

1157 GROMACS/EE and GROMACS/EE-fullequil

1158 The free energy of bindings were obtained with the double decoupling method [15] using the expanded
1159 ensemble enhanced-sampling methodology [21] implemented in GROMACS 2018.3 [73]. Charges were
1160 turned off completely before removing Van der Waals interactions in both the complex and the solvent
1161 phase. Both Coulomb and Lennard-Jones interactions were annihilated (i.e. intra-molecular interactions
1162 were turned off). Two restraints were used during the complex phase of the calculation: a flat-bottom
1163 restraint with radius 1.5 nm and spring constant 1000 kJ/mol-nm², and a harmonic restraint with spring
1164 constant 1000 kJ/mol-nm². Both restraints were attached to the centers of mass of host and guest, but while
1165 the flat-bottom restraint remained throughout the simulation, the harmonic restraint was incrementally
1166 activated while the Lennard-Jones interactions were removed. In the bound state, the flat-bottom distance
1167 between the centers of mass remained always smaller than the 1.5 nm radius necessary to have a non-zero
1168 potential.

1169 Because of instabilities and bias introduced by the Berendsen barostat during the expanded ensem-
1170 ble calculation, all the simulations were performed in NVT using the average volume sampled by the
1171 OpenMM/HREX calculations performed with YANK. V-rescale temperature was used to keep the temperature
1172 at 298.15 K, and and bonds to hydrogen atoms were constrained using the SHAKE algorithm. We used the
1173 md-vv integrator, a velocity Verlet integrator, with time steps of 2 fs. Metropolized Gibbs Monte Carlo moves
1174 between all intermediate states [82] were performed every 100 time steps based on weights calculated
1175 with the Wang-Landau (WL) algorithm as described below. The metropolized Gibbs move in state space
1176 proposes jumps to all states except the current state, with a rejection step to satisfy detailed balance. An
1177 equal number of time steps were allocated to production simulations of complex and solvent systems for
1178 each free energy estimate. A cutoff of 10Å was used for nonbonded interactions with a switching function
1179 between 9 Å and 10 Å for Lennard-Jones forces. Particle Mesh Ewald used an interpolation order of 5 and a

1180 tolerance of 10^{-5} . A sample .mdp file can be found in the submission at https://github.com/samplchallenges/SAMPL6/blob/master/host_guest/Analysis/Submissions/SAMPLing/NB006-975-absolute-EENV-1.txt.

1182 The expanded ensemble calculation was divided into two stages: an equilibration stage, in which the
1183 expanded ensemble weights were adaptively estimated, and a production stage that generated the data
1184 used to compute the submitted free energy estimates and in which the weights were kept fixed. In the
1185 equilibration stage, the weights are adaptively estimated using the Wang-Landau algorithm [83, 84]. For all
1186 systems an absolute value of the initial Wang-Landau incrementor was set to $2 k_B T$. Weights were updated at
1187 each step, and the increment amount was reduced by a factor of 0.8 each time a flat histogram was observed,
1188 meaning that the ratio between the least visited and most visited states since the last change in the weight
1189 increment was less than 0.7. The process of updating the weights was halted when the incrementing amount
1190 fell below $0.001 k_B T$. Equilibration of the weights was only ran on a single starting conformation out of five
1191 for each host-guest pair. The weight of the fully coupled state is normalized to zero, meaning that the weight
1192 of the uncoupled state corresponds to the free energy of the process. The last stage of the simulation,
1193 during which period the expanded ensemble weights were no longer updated, was termed the "production"
1194 stage since it was the only part of the trajectory used to calculate the final free energy change. Once the
1195 Wang-Landau incrementor reached a value of $0.001 k_B T$ the simulation was stopped, MBAR was ran on
1196 simulation data obtained while the Wang-Landau incrementor was between values of 0.01 and $0.001 k_B T$,
1197 and the resulting free energies were used to set the weights for the production simulations for all starting
1198 conformation of a host-guest pair.

1199 Reported values were obtained by running MBAR on production simulation data. The submissions
1200 GROMACS/EE and GROMACS/EE-fullequil differ only in whether the computational cost of the equilibration
1201 is added in its entirety to each of the five replicate calculations (GROMACS/EE-fullequil) or whether it is
1202 amortized over the replicates (GROMACS/EE).

1203 NAMD/BAR

1204 The alchemical free energy calculations were performed using the double decoupling method as imple-
1205 mented in NAMD 2.12 [74]. The NAMD protocol utilized a total number of 32 equidistant λ windows, that are
1206 simulated independently for 20 ns/window with Langevin dynamics using a 2 fs time step and coupling coef-
1207 ficient of 1.0 ps^{-1} . The Lennard-Jones interactions are linearly decoupled from the simulation in equidistant
1208 windows between 0 and 1, while the charges were turned off together with LJ over the λ values 0-0.9 for
1209 CB8-G3 and 0-0.5 for OA-G3 and OA-G6. During the complex leg of the simulation a flat-bottom restraint
1210 with a wall constant of $100 \text{ kcal/mol/\AA}^2$ was applied to prevent the guest from drifting away from the host.
1211 A non-interacting particle having the same charge of the guest was created during the annihilation of the
1212 Coulomb interactions in order to maintain the charge neutrality of the box [65, 89]. Before collecting samples
1213 for the free energy estimation, each window was equilibrated for 2 ns. The pressure was maintained at
1214 1 atm using a modified Nosé-Hoover method implemented in NAMD, in which Langevin dynamics is used to
1215 control fluctuations in the barostat [130, 131]. The Langevin piston utilized an oscillation period of 100 fs
1216 and a damping time scale of 50 fs. Long range electrostatic interactions were treated with the following
1217 PME parameters: PME tolerance = 10^{-6} , PME spline order 4, and PME grid = $48 \times 48 \times 48$. The cutoff for both
1218 Lennard-Jones and PME was set to 10 \AA , and the switching distance was set to 9 \AA . The free energy of each
1219 replicate calculation and their uncertainties were computed with BAR using ParseFEP [132] Tcl plugin (version
1220 2.1) for VMD 1.9.4a29.

1221 OpenMM/HREX

1222 The free energy calculations and analysis were performed with YANK 0.20.1 [79, 80] and OpenMMTools
1223 0.14.0 [124] powered by OpenMM 7.2.0 [75]. The protocol followed the double decoupling methodology [15]
1224 using the thermodynamic cycle in SI Figure 4. In both phases, we first annihilated the guest charges (i.e.
1225 intra-molecular electrostatics was turned off) and then decoupled the soft-core (1-1-6 model) Lennard Jones
1226 interactions [81] (i.e. intra-molecular sterics was left untouched). The spacing and number of intermediate
1227 states was determined automatically for the three systems by the trailblaze algorithm implemented in
1228 YANK [79]. This resulted in a protocol with a total of 69 and 62 intermediate states for the complex and

1229 solvent phase respectively of CB8-G3, 59 and 54 states for OA-G3, and 55 and 52 states for OA-G6. Since all
1230 guests had a net charge, a counterion of opposite charge was decoupled with the guest to maintain the box
1231 neutrality at each intermediate state and avoid artifacts introduced by finite-size effects with Particle Mesh
1232 Ewald.

1233 Hamiltonian replica exchange [20] was used to enhance sampling of the binding modes. Each iteration
1234 of the algorithm was composed by a metropolized rigid translation, using a Gaussian proposal of mean 0
1235 and standard deviation 1 nm, and a random rotation of the ligand followed by 1 ps of Langevin dynamics
1236 (BAOAB splitting [22], 2 fs timestep, 10/ps collision rate). A Monte Carlo barostat step was performed every
1237 25 integration steps to maintain a pressure of 1 atm. All hydrogen bonds were constrained. The Hamiltonian
1238 exchange step was carried out after each iteration by performing K^4 metropolized Gibbs sampling steps [82],
1239 where K is the number of intermediate states in the protocol. At the beginning of each iteration, velocities
1240 for all replicas were randomly re-sampled from the Boltzmann distribution. In all calculations, we ran 40000
1241 iterations of the algorithm (i.e. 40 ns of MD per replica) for both the complex and solvent calculation for a
1242 total MD propagation of 5.24 μ s, 4.52 μ s, and 4.28 μ s for each of the five replicates of CB8-G3, OA-G3, and
1243 OA-G6 respectively. An analytical dispersion correction for the long-range Lennard-Jones interactions was
1244 added during the simulation for all atoms except the alchemically-softened atoms for optimization reason.
1245 The contribution of the guest to the dispersion correction was instead found by reweighting the end states.

1246 The analysis of the samples was performed with the MBAR estimator [78] with PyMBAR 3.0.3. We
1247 computed an estimate of the statistical inefficiency of the sampling process in order to decorrelate the
1248 HREX samples. The statistical inefficiency was estimated from the correlation function of the time series of
1249 the traces of the $K \times K$ MBAR energy matrix $U(i)$ computed at each iteration i , where the matrix element
1250 $U_{jl}(i)$ is the reduced potential of the sample generated by state j at iteration i and evaluated in state l . The
1251 resulting statistical inefficiencies were 2.74 ± 0.03 ps, 2.9 ± 0.3 ps, and 2.84 ± 0.3 ps for CB8-G3, OA-G3,
1252 and OA-G6 respectively (uncertainties are given as the standard deviation of the statistical inefficiencies
1253 over replicates). The statistical inefficiency was then used to discard the burn-in data by maximizing the
1254 number of effective samples as described in [133] and to subsample the data before running MBAR. In
1255 the complex phase, the guest was restrained throughout the calculation into the binding site through a
1256 single harmonic restraint connecting the center of mass of the heavy atoms of host and guest with a spring
1257 constant of 0.2 kcal/(mol \cdot \AA^2) for CB8-G3 and 0.17 (mol \cdot \AA^2) for OA-G3/G6. Following the double decoupling
1258 approach, an analytical correction was added to bring the affinity in units of standard concentration and
1259 correct for the restraint volume in the decoupled state. However, because the restraint was activated
1260 in the bound state as well, we also used MBAR to reweight the samples to remove the bias introduced
1261 by the harmonic potential. Samples whose restrained distance (i.e. the distance between the host and
1262 guest centers of mass) was above a specific threshold were discarded. This is equivalent to reweighting
1263 the data to a state having a restraint following a square well potential, where the energy is either zero
1264 or infinity, with a radius equal to the distance threshold. The distance threshold was determined by
1265 selecting the 99.99-percentile distance sampled in the bound state, which resulted in 4.5830673 \AA for CB8-G3,
1266 5.773037 \AA for OA-G3, and 6.0628217 \AA for OA-G6. The YANK input file used for the calculation can be found
1267 at https://github.com/samplchallenges/SAMPL6/blob/master/host_guest/SAMPLing/YANK_input_script.yaml.

1268 The number of energy evaluations used to determine the computational cost of the method was
1269 computed for each iteration as $MD_{cost} + MC_{cost} + MBAR_{cost}$, where MD_{cost} is the number of force evaluations
1270 used to propagate the system (i.e. 1 ps/2 fs = 500 force evaluations), MC_{cost} are the number of energy
1271 evaluations performed for acceptance/rejection of the MC rotation and translation (4 energy evaluations),
1272 and $MBAR_{cost}$ is the number of energy evaluations necessary to compute the MBAR free energy matrix at
1273 each iteration. We set $MBAR_{cost} = K \times K$, where K is both the number of states and the number of replicas.
1274 This is an overestimation as YANK computes the energies of each replica for all states by recomputing only
1275 the parts of the Hamiltonian that change from state to state.

1276 6.3 Estimation of the relative efficiency

1277 We considered the standard deviation, absolute bias, and RMSE error statistics in Eq. (2, 4) to compute
1278 respectively the relative efficiencies e_{std} , e_{bias} , e_{RMSE} . The relative efficiencies of all methods were estimated

1279 with respect to OpenMM/HREX, which was the longest calculation and could provide free energy predictions
1280 at all the computational costs intervals required to estimate the statistics. We used a uniform weight
1281 $w(c) = \text{const.}$ for all methods, and, because we have data available for only 100 computational costs over
1282 the interval $[c_{\min,X}, c_{\max,X}]$, we interpolated the error statistic for the other values of c and approximated the
1283 average over the number of energy evaluations with

$$\mathbb{E}_w[\text{err}_X(c)] = \frac{1}{c_{\max,X} - c_{\min,X} + 1} \sum_{c=c_{\min,X}}^{c_{\max,X}} \text{err}_X(c) \approx \frac{1}{c_{\max,X} - c_{\min,X}} \text{trapz}(\text{err}_X(c), c_{\min,X}, c_{\max,X}) \quad (6)$$

1284 where $\text{trapz}(\cdot)$ represent the quadrature integral of the error function performed with the trapezoidal rule
1285 over the considered interval of c . The denominator does not affect the relative efficiency as it cancels out in
1286 Eq. (5).

The population mean $\mathbb{E}[\Delta G(c)]$ and standard deviation $\text{std}(\Delta G(c))$ of the binding free energy predictions at computational cost c were estimated as usual with the sample mean $\overline{\Delta G(c)}$ and the sample standard deviation $S(c)$ respectively calculated using the five independent replicates

$$\begin{aligned} \overline{\Delta G(c)} &= \frac{1}{N_c} \sum_{j=1}^{N_c} \Delta G^{(j)}(c) \\ S(c) &= \sqrt{\frac{1}{N_c - 1} \sum_{j=1}^{N_c} [\Delta G^{(j)}(c) - \overline{\Delta G(c)}]^2} \end{aligned} \quad (7)$$

1287 where $N_c = 5$ is the number of independent measures at computational cost c .

1288 However, estimating the error statistics defined in Eq. (2, 4) requires estimates of the asymptotic free
1289 energy ΔG_θ , which is necessary for the bias. This is problematic due to the different levels of convergence
1290 and the lack of agreement between methods. We estimated the bias assuming $\Delta G_{\theta,X} = \overline{\Delta G_X(c_{\max,X})}$, where
1291 $c_{\max,X}$ is the total computational cost of the calculation for method X , which is equivalent to assuming that
1292 the free energy estimate has converged. As a consequence, the bias is generally underestimated, and longer
1293 calculations are penalized in computing the relative absolute bias and RMSE efficiency.

1294 To estimate 95% confidence intervals for the relative efficiency measures we used the `arch` 4.6.0 Python
1295 library [134] to run the bias-corrected and accelerated (BCa) bootstrap method by resampling free energy
1296 trajectories with replacement. The acceleration parameter was estimated with the jackknife method.

1297 Code and data availability

- 1298 • Input files and setup scripts: https://github.com/samplchallenges/SAMPL6/tree/master/host_guest/SAMPLing/
- 1299
- 1300 • Analysis scripts: https://github.com/samplchallenges/SAMPL6/tree/master/host_guest/Analysis/Scripts/
- 1301 • Analysis results: https://github.com/samplchallenges/SAMPL6/tree/master/host_guest/Analysis/SAMPLing/
- 1302 • Participant submissions: [https://github.com/samplchallenges/SAMPL6/tree/master/host_guest/Analysis/](https://github.com/samplchallenges/SAMPL6/tree/master/host_guest/Analysis/Submissions/SAMPLing/)
- 1303 [Submissions/SAMPLing/](https://github.com/samplchallenges/SAMPL6/tree/master/host_guest/Analysis/Submissions/SAMPLing/)

1304 Author Contributions

1305 Conceptualization: DLM, AR, JDC, MS, JM; Data Curation: AR; Formal Analysis: AR; Funding Acquisition: JDC,
1306 DLM, MRS, MKG, AD, BLdG, JM, ZC; Investigation: AR, TJ, DRS, MA, VG, AD, DN, SB, NMH, MP; Methodology:
1307 AR, DLM, MKG, JM, JDC; Project Administration: AR, DLM, JDC; Resources: JDC, MRS, MKG, ZC, JM, AD, BLdG;
1308 Software: AR; Supervision: JDC, MRS, MKG, DLM, JM, ZC, AD, BLdG; Visualization: AR, VG, TJ; Writing – Original
1309 Draft: AR; Writing – Review & Editing: AR, MKG, JDC, DLM, DRS, MRS, MA, VG, JM, DN, AD, ZC, BLdG.

1310 Acknowledgments

1311 AR and JDC acknowledge support from the Sloan Kettering Institute. JDC acknowledges support from NIH
1312 grant P30 CA008748. AR acknowledges partial support from the Tri-Institutional Program in Computa-
1313 tional Biology and Medicine. DLM appreciates financial support from the National Institutes of Health

1314 (1R01GM108889-01 and 1R01GM124270-01A1) and the National Science Foundation (CHE 1352608). AR and
1315 JDC are grateful to OpenEye Scientific for providing a free academic software license for use in this work. MA
1316 was supported by a Postdoctoral Research Fellowship of the Alexander von Humboldt Foundation. VG and
1317 BLdG were supported by BioExcel CoE, a project funded by the European Union contract H2020-INFRAEDI-
1318 02-2018-823830. MKG thanks NIGMS (NIH) for partial support of this project (GM061300). The contents
1319 of this publication are solely the responsibility of the authors and do not necessarily represent the official
1320 views of the NIH. AD acknowledges support from the National Institutes of Health (R01GM130794) and the
1321 National Science Foundation (DMS 1761320). ZC and DN would like to thank Stamatia Zavitsanou, Michail
1322 Papadourakis and Chris Chipot for useful discussions. This work was further supported by computational
1323 time granted from the Greek Research & Technology Network (GRNET) in the National HPC facility - ARIS-
1324 under project ID vspr001005/arp2/3. ZC acknowledges support of this work by the project "An Open-Access
1325 Research Infrastructure of Chemical Biology and Target-Based Screening Technologies for Human and Animal
1326 Health, Agriculture and the Environment (OPENSREEN-GR)" (MIS 5002691), which is implemented under the
1327 Action "Reinforcement of the Research and Innovation Infrastructure", funded by the Operational Programme
1328 "Competitiveness, Entrepreneurship and Innovation" (NSRF 2014-2020) and co-financed by Greece and the
1329 European Union (European Regional Development Fund).

1330 Disclosures

1331 JDC was a member of the Scientific Advisory Board for Schrödinger, LLC during part of this study. JDC and
1332 DLM are current members of the Scientific Advisory Board of OpenEye Scientific Software. The Chodera
1333 laboratory receives or has received funding from multiple sources, including the National Institutes of Health,
1334 the National Science Foundation, the Parker Institute for Cancer Immunotherapy, Relay Therapeutics, Entasis
1335 Therapeutics, Silicon Therapeutics, EMD Serono (Merck KGaA), AstraZeneca, Vir Biotechnology, XtalPi, the
1336 Molecular Sciences Software Institute, the Starr Cancer Consortium, the Open Force Field Consortium, Cycle
1337 for Survival, a Louis V. Gerstner Young Investigator Award, and the Sloan Kettering Institute. A complete
1338 funding history for the Chodera lab can be found at <http://choderalab.org/funding>. MKG has an equity
1339 interest in, and is a cofounder and scientific advisor of VeraChem LLC.

1340 References

- 1341 [1] **Shirts MR**, Mobley DL, Brown SP. Free-energy calculations in structure-based drug design. *Drug design: structure-*
1342 *and ligand-based approaches*. 2010; p. 61–86.
- 1343 [2] **Kuhn B**, Tichý M, Wang L, Robinson S, Martin RE, Kuglstatter A, Benz J. Prospective evaluation of free energy
1344 calculations for the prioritization of cathepsin L inhibitors. *Journal of medicinal chemistry*. 2017; 60(6):2485–2497.
- 1345 [3] **Ciordia M**, Pérez-Benito L, Delgado F, Trabanco AA, Tresadern G. Application of free energy perturbation for the
1346 design of BACE1 inhibitors. *Journal of Chemical information and modeling*. 2016; 56(9):1856–1871.
- 1347 [4] **Schindler C**, Rippmann F, Kuhn D. Relative binding affinity prediction of farnesoid X receptor in the D3R Grand
1348 Challenge 2 using FEP+. *Journal of computer-aided molecular design*. 2018; 32(1):265–272.
- 1349 [5] **Wang L**, Wu Y, Deng Y, Kim B, Pierce L, Krilov G, Lupyan D, Robinson S, Dahlgren MK, Greenwood J, et al. Accurate and
1350 reliable prediction of relative ligand binding potency in prospective drug discovery by way of a modern free-energy
1351 calculation protocol and force field. *Journal of the American Chemical Society*. 2015; 137(7):2695–2703.
- 1352 [6] **Minh DD**. Alchemical Grid Dock (AIGDock): Binding Free Energy Calculations between Flexible Ligands and Rigid
1353 Receptors. *Journal of Computational Chemistry*. 2019; .
- 1354 [7] **Capelli R**, Carloni P, Parrinello M. Exhaustive Search of Ligand Binding Pathways via Volume-based Metadynamics.
1355 *The journal of physical chemistry letters*. 2019; .
- 1356 [8] **Irwin BW**, Huggins DJ. Estimating atomic contributions to hydration and binding using free energy perturbation.
1357 *Journal of chemical theory and computation*. 2018; 14(6):3218–3227.
- 1358 [9] **Sherborne B**, Shanmugasundaram V, Cheng AC, Christ CD, Desjarlais RL, Duca JS, Lewis RA, Loughney DA, Manas
1359 ES, McGaughey GB, et al. Collaborating to improve the use of free-energy and other quantitative methods in drug
1360 discovery. *Journal of computer-aided molecular design*. 2016; 30(12):1139–1141.

- 1361 [10] **Cournia Z**, Allen B, Sherman W. Relative binding free energy calculations in drug discovery: recent advances and
1362 practical considerations. *Journal of chemical information and modeling*. 2017; 57(12):2911–2937.
- 1363 [11] **Mobley DL**, Gilson MK. Predicting binding free energies: frontiers and benchmarks. *Annual review of biophysics*.
1364 2017; 46:531–558.
- 1365 [12] **Gathiaka S**, Liu S, Chiu M, Yang H, Stuckey JA, Kang YN, Delproposto J, Kubish G, Dunbar JB, Carlson HA, et al.
1366 D3R grand challenge 2015: evaluation of protein–ligand pose and affinity predictions. *Journal of computer-aided*
1367 *molecular design*. 2016; 30(9):651–668.
- 1368 [13] **Gaieb Z**, Liu S, Gathiaka S, Chiu M, Yang H, Shao C, Feher VA, Walters WP, Kuhn B, Rudolph MG, et al. D3R Grand
1369 Challenge 2: blind prediction of protein–ligand poses, affinity rankings, and relative binding free energies. *Journal of*
1370 *computer-aided molecular design*. 2018; 32(1):1–20.
- 1371 [14] **Gaieb Z**, Parks CD, Chiu M, Yang H, Shao C, Walters WP, Lambert MH, Nevins N, Bembenek SD, Ameriks MK, et al.
1372 D3R Grand Challenge 3: blind prediction of protein–ligand poses and affinity rankings. *Journal of computer-aided*
1373 *molecular design*. 2019; 33(1):1–18.
- 1374 [15] **Gilson MK**, Given JA, Bush BL, McCammon JA. The statistical-thermodynamic basis for computation of binding
1375 affinities: a critical review. *Biophysical journal*. 1997; 72(3):1047–1069. doi: [10.1016/S0006-3495\(97\)78756-3](https://doi.org/10.1016/S0006-3495(97)78756-3).
- 1376 [16] **Laio A**, Parrinello M. Escaping free-energy minima. *Proceedings of the National Academy of Sciences*. 2002;
1377 99(20):12562–12566.
- 1378 [17] **Barducci A**, Bussi G, Parrinello M. Well-tempered metadynamics: a smoothly converging and tunable free-energy
1379 method. *Physical review letters*. 2008; 100(2):020603.
- 1380 [18] **Swendsen RH**, Wang JS. Replica Monte Carlo simulation of spin-glasses. *Physical review letters*. 1986; 57(21):2607.
- 1381 [19] **Hukushima K**, Nemoto K. Exchange Monte Carlo method and application to spin glass simulations. *Journal of the*
1382 *Physical Society of Japan*. 1996; 65(6):1604–1608.
- 1383 [20] **Sugita Y**, Kitao A, Okamoto Y. Multidimensional replica-exchange method for free-energy calculations. *The Journal*
1384 *of Chemical Physics*. 2000; 113(15):6042–6051. doi: [10.1063/1.1308516](https://doi.org/10.1063/1.1308516).
- 1385 [21] **Lyubartsev A**, Martsinovski A, Shevkunov S, Vorontsov-Velyaminov P. New approach to Monte Carlo calculation of
1386 the free energy: Method of expanded ensembles. *The Journal of chemical physics*. 1992; 96(3):1776–1783.
- 1387 [22] **Leimkuhler B**, Matthews C. Rational construction of stochastic numerical methods for molecular sampling. *Applied*
1388 *Mathematics Research eXpress*. 2012; 2013(1):34–56.
- 1389 [23] **Fass J**, Sivak D, Crooks G, Beauchamp K, Leimkuhler B, Chodera J. Quantifying configuration-sampling error in
1390 Langevin simulations of complex molecular systems. *Entropy*. 2018; 20(5):318.
- 1391 [24] **Shirts MR**, Pande VS. Comparison of efficiency and bias of free energies computed by exponential averaging, the
1392 Bennett acceptance ratio, and thermodynamic integration. *The Journal of chemical physics*. 2005; 122(14):144107.
- 1393 [25] **Yin J**, Henriksen NM, Slochower DR, Shirts MR, Chiu MW, Mobley DL, Gilson MK. Overview of the SAMPL5 host–guest
1394 challenge: Are we doing better? *Journal of computer-aided molecular design*. 2017; 31(1):1–19.
- 1395 [26] **Rizzi A**, Murkli S, McNeill JN, Yao W, Sullivan M, Gilson MK, Chiu MW, Isaacs L, Gibb BC, Mobley DL, et al. Overview of
1396 the SAMPL6 host–guest binding affinity prediction challenge. *Journal of computer-aided molecular design*. 2018;
1397 32(10):937–963.
- 1398 [27] **Cabeza de Vaca I**, Qian Y, Vilseck JZ, Tirado-Rives J, Jorgensen WL. Enhanced Monte Carlo Methods for Modeling
1399 Proteins Including Computation of Absolute Free Energies of Binding. *Journal of chemical theory and computation*.
1400 2018; 14(6):3279–3288.
- 1401 [28] **Deng N**, Cui D, Zhang BW, Xia J, Cruz J, Levy R. Comparing alchemical and physical pathway methods for computing
1402 the absolute binding free energy of charged ligands. *Physical Chemistry Chemical Physics*. 2018; 20(25):17081–
1403 17092.
- 1404 [29] **Shirts MR**, Klein C, Swails JM, Yin J, Gilson MK, Mobley DL, Case DA, Zhong ED. Lessons learned from comparing
1405 molecular dynamics engines on the SAMPL5 dataset. *Journal of computer-aided molecular design*. 2016; p. 1–15.
1406 doi: [doi:10.1007/s10822-016-9977-1](https://doi.org/10.1007/s10822-016-9977-1).

- 1407 [30] **Loeffler HH**, Bosisio S, Duarte Ramos Matos G, Suh D, Roux B, Mobley DL, Michel J. Reproducibility of free energy
1408 calculations across different molecular simulation software packages. *Journal of chemical theory and computation*.
1409 2018; 14(11):5567–5582.
- 1410 [31] **Aldeghi M**, Heifetz A, Bodkin MJ, Knapp S, Biggin PC. Accurate calculation of the absolute free energy of binding for
1411 drug molecules. *Chemical science*. 2016; 7(1):207–218.
- 1412 [32] **Bhati AP**, Wan S, Wright DW, Coveney PV. Rapid, accurate, precise, and reliable relative free energy prediction using
1413 ensemble based thermodynamic integration. *Journal of chemical theory and computation*. 2016; 13(1):210–222.
- 1414 [33] **Xie B**, Nguyen TH, Minh DD. Absolute binding free energies between T4 lysozyme and 141 small molecules:
1415 calculations based on multiple rigid receptor configurations. *Journal of chemical theory and computation*. 2017;
1416 13(6):2930–2944.
- 1417 [34] **Henriksen NM**, Gilson MK. Evaluating force field performance in thermodynamic calculations of cyclodextrin
1418 host–guest binding: Water models, partial charges, and host force field parameters. *Journal of chemical theory and
1419 computation*. 2017; 13(9):4253–4269.
- 1420 [35] **Gill SC**, Lim NM, Grinaway PB, Rustenburg AS, Fass J, Ross GA, Chodera JD, Mobley DL. Binding Modes of Ligands
1421 Using Enhanced Sampling (BLUES): Rapid Decorrelation of Ligand Binding Modes via Nonequilibrium Candidate
1422 Monte Carlo. *The Journal of Physical Chemistry B*. 2018; 122(21):5579–5598.
- 1423 [36] **Miao Y**, Feher VA, McCammon JA. Gaussian accelerated molecular dynamics: Unconstrained enhanced sampling
1424 and free energy calculation. *Journal of chemical theory and computation*. 2015; 11(8):3584–3595.
- 1425 [37] **Pham TT**, Shirts MR. Optimal pairwise and non-pairwise alchemical pathways for free energy calculations of
1426 molecular transformation in solution phase. *The Journal of chemical physics*. 2012; 136(12):124120.
- 1427 [38] **Athènes M**, Terrier P. Estimating thermodynamic expectations and free energies in expanded ensemble simulations:
1428 Systematic variance reduction through conditioning. *The Journal of chemical physics*. 2017; 146(19):194101.
- 1429 [39] **Nguyen TH**, Minh DD. Intermediate Thermodynamic States Contribute Equally to Free Energy Convergence: A
1430 Demonstration with Replica Exchange. *Journal of chemical theory and computation*. 2016; 12(5):2154–2161.
- 1431 [40] **Shenfeld DK**, Xu H, Eastwood MP, Dror RO, Shaw DE. Minimizing thermodynamic length to select intermediate
1432 states for free-energy calculations and replica-exchange simulations. *Physical Review E*. 2009; 80(4):046705.
- 1433 [41] **MacCallum JL**, Muniyat MI, Gaalswyk K. Online optimization of total acceptance in Hamiltonian replica exchange
1434 simulations. *The Journal of Physical Chemistry B*. 2018; 122(21):5448–5457.
- 1435 [42] **Lindahl V**, Lidmar J, Hess B. Riemann metric approach to optimal sampling of multidimensional free-energy
1436 landscapes. *Physical Review E*. 2018; 98(2):023312.
- 1437 [43] **Martinsson A**, Lu J, Leimkuhler B, Vanden-Eijnden E. The simulated tempering method in the infinite switch limit
1438 with adaptive weight learning. *Journal of Statistical Mechanics: Theory and Experiment*. 2019; 2019(1):013207.
- 1439 [44] **Crooks GE**. Measuring thermodynamic length. *Physical Review Letters*. 2007; 99(10):100602.
- 1440 [45] **Sivak DA**, Crooks GE. Thermodynamic metrics and optimal paths. *Physical review letters*. 2012; 108(19):190602.
- 1441 [46] **Coleman RG**, Sterling T, Weiss DR. SAMPL4 & DOCK3. 7: lessons for automated docking procedures. *Journal of
1442 computer-aided molecular design*. 2014; 28(3):201–209.
- 1443 [47] **Eken Y**, Patel P, Díaz T, Jones MR, Wilson AK. SAMPL6 host–guest challenge: binding free energies via a multistep
1444 approach. *Journal of computer-aided molecular design*. 2018; 32(10):1097–1115.
- 1445 [48] **Hudson PS**, Han K, Woodcock HL, Brooks BR. Force matching as a stepping stone to QM/MM CB [8] host/guest
1446 binding free energies: a SAMPL6 cautionary tale. *Journal of computer-aided molecular design*. 2018; 32(10):983–999.
- 1447 [49] **Olsson MA**, Ryde U. Comparison of QM/MM methods to obtain ligand-binding free energies. *Journal of chemical
1448 theory and computation*. 2017; 13(5):2245–2253.
- 1449 [50] **Zheng Z**, Ucisik MN, Merz KM. The movable type method applied to protein–ligand binding. *Journal of chemical
1450 theory and computation*. 2013; 9(12):5526–5538.
- 1451 [51] **Bansal N**, Zheng Z, Cerutti DS, Merz KM. On the fly estimation of host–guest binding free energies using the
1452 movable type method: participation in the SAMPL5 blind challenge. *Journal of computer-aided molecular design*.
1453 2017; 31(1):47–60.

- 1454 [52] **Organization WH**. Guidelines for the treatment of malaria. World Health Organization; 2015.
- 1455 [53] **Gibb CL**, Gibb BC. Well-defined, organic nanoenvironments in water: The hydrophobic effect drives a capsular
1456 assembly. *Journal of the American Chemical Society*. 2004; 126(37):11408–11409.
- 1457 [54] **Hillyer MB**, Gibb CL, Sökkalingam P, Jordan JH, Ioup SE, Gibb BC. Synthesis of water-soluble deep-cavity cavitands.
1458 *Organic letters*. 2016; 18(16):4048–4051.
- 1459 [55] **Liu S**, Ruspic C, Mukhopadhyay P, Chakrabarti S, Zavalij PY, Isaacs L. The cucurbit [n] uril family: prime components
1460 for self-sorting systems. *Journal of the American Chemical Society*. 2005; 127(45):15959–15967.
- 1461 [56] **Mobley DL**, Heinzelmann G, Henriksen NM, Gilson MK. Predicting binding free energies: Frontiers and benchmarks
1462 (a perpetual review). UC Irvine: Department of Pharmaceutical Sciences, UCI. 2017; [https://escholarship.org/uc/](https://escholarship.org/uc/item/9p37m6bq)
1463 [item/9p37m6bq](https://escholarship.org/uc/item/9p37m6bq).
- 1464 [57] **Muddana HS**, Gilson MK. Prediction of SAMPL3 host–guest binding affinities: evaluating the accuracy of generalized
1465 force-fields. *Journal of computer-aided molecular design*. 2012; 26(5):517–525.
- 1466 [58] **Muddana HS**, Fenley AT, Mobley DL, Gilson MK. The SAMPL4 host–guest blind prediction challenge: an overview.
1467 *Journal of computer-aided molecular design*. 2014; 28(4):305–317.
- 1468 [59] **Ewell J**, Gibb BC, Rick SW. Water inside a hydrophobic cavitand molecule. *The Journal of Physical Chemistry B*. 2008;
1469 112(33):10272–10279.
- 1470 [60] **Rogers KE**, Ortiz-Sánchez JM, Baron R, Fajer M, de Oliveira CAF, McCammon JA. On the role of dewetting transitions
1471 in host–guest binding free energy calculations. *Journal of chemical theory and computation*. 2012; 9(1):46–53. doi:
1472 [10.1021/ct300515n](https://doi.org/10.1021/ct300515n).
- 1473 [61] **Mobley DL**, Chodera JD, Dill KA. On the use of orientational restraints and symmetry corrections in alchemical free
1474 energy calculations. *The Journal of chemical physics*. 2006; 125(8):084902.
- 1475 [62] **Chen W**, Deng Y, Russell E, Wu Y, Abel R, Wang L. Accurate calculation of relative binding free energies between
1476 ligands with different net charges. *Journal of chemical theory and computation*. 2018; 14(12):6346–6358.
- 1477 [63] **Rocklin GJ**, Mobley DL, Dill KA, Hünenberger PH. Calculating the binding free energies of charged species based
1478 on explicit-solvent simulations employing lattice-sum methods: An accurate correction scheme for electrostatic
1479 finite-size effects. *The Journal of chemical physics*. 2013; 139(18):11B606_1.
- 1480 [64] **Lin YL**, Aleksandrov A, Simonson T, Roux B. An overview of electrostatic free energy computations for solutions and
1481 proteins. *Journal of chemical theory and computation*. 2014; 10(7):2690–2709.
- 1482 [65] **Morgan BR**, Massi F. Accurate estimates of free energy changes in charge mutations. *Journal of chemical theory*
1483 *and computation*. 2010; 6(6):1884–1893.
- 1484 [66] **McGann M**. FRED pose prediction and virtual screening accuracy. *Journal of chemical information and modeling*.
1485 2011; 51(3):578–596. doi: [10.1021/ci100436p](https://doi.org/10.1021/ci100436p).
- 1486 [67] **McGann M**. FRED and HYBRID docking performance on standardized datasets. *Journal of computer-aided molecular*
1487 *design*. 2012; 26(8):897–906. doi: [10.1007/s10822-012-9584-8](https://doi.org/10.1007/s10822-012-9584-8).
- 1488 [68] **Jakalian A**, Bush BL, Jack DB, Bayly CI. Fast, efficient generation of high-quality atomic Charges. AM1-
1489 BCC model: I. Method. *Journal of computational chemistry*. 2000; 21(2):132–146. doi: [10.1002/\(SICI\)1096-](https://doi.org/10.1002/(SICI)1096-987X(20000130)21:2<132::AID-JCC5>3.0.CO;2-P)
1490 [987X\(20000130\)21:2<132::AID-JCC5>3.0.CO;2-P](https://doi.org/10.1002/(SICI)1096-987X(20000130)21:2<132::AID-JCC5>3.0.CO;2-P).
- 1491 [69] **Jakalian A**, Jack DB, Bayly CI. Fast, efficient generation of high-quality atomic charges. AM1-BCC model: II. Parame-
1492 terization and validation. *Journal of computational chemistry*. 2002; 23(16):1623–1641. doi: [10.1002/jcc.10128](https://doi.org/10.1002/jcc.10128).
- 1493 [70] **Wang J**, Wolf RM, Caldwell JW, Kollman PA, Case DA. Development and testing of a general amber force field. *Journal*
1494 *of computational chemistry*. 2004; 25(9):1157–1174. doi: [10.1002/jcc.20035](https://doi.org/10.1002/jcc.20035).
- 1495 [71] **Jorgensen WL**, Chandrasekhar J, Madura JD, Impey RW, Klein ML. Comparison of simple potential functions for
1496 simulating liquid water. *The Journal of chemical physics*. 1983; 79(2):926–935. doi: [10.1063/1.445869](https://doi.org/10.1063/1.445869).
- 1497 [72] **Case D**, Ben-Shalom I, Brozell S, Cerutti D, Cheatham T, III, Cruzeiro V, Darden T, Duke R, Ghoreishi D, Gilson M,
1498 Gohlke H, Goetz A, Greene D, Harris R, Homeyer N, Izadi S, Kovalenko A, Kurtzman T, Lee T, et al., AMBER 18; 2018.
1499 University of California, San Francisco.

- 1500 [73] **Abraham MJ**, Murtola T, Schulz R, Páll S, Smith JC, Hess B, Lindahl E. GROMACS: High performance molecular
1501 simulations through multi-level parallelism from laptops to supercomputers. *SoftwareX*. 2015; 1:19–25.
- 1502 [74] **Phillips JC**, Braun R, Wang W, Gumbart J, Tajkhorshid E, Villa E, Chipot C, Skeel RD, Kale L, Schulten K. Scalable
1503 molecular dynamics with NAMD. *Journal of computational chemistry*. 2005; 26(16):1781–1802.
- 1504 [75] **Eastman P**, Swails J, Chodera JD, McGibbon RT, Zhao Y, Beauchamp KA, Wang LP, Simmonett AC, Harrigan MP,
1505 Stern CD, et al. OpenMM 7: rapid development of high performance algorithms for molecular dynamics. *PLoS*
1506 *computational biology*. 2017; 13(7):e1005659. doi: [10.1371/journal.pcbi.1005659](https://doi.org/10.1371/journal.pcbi.1005659).
- 1507 [76] **Papadourakis M**, Bosisio S, Michel J. Blinded predictions of standard binding free energies: lessons learned from
1508 the SAMPL6 challenge. *Journal of computer-aided molecular design*. 2018; 32(10):1047–1058.
- 1509 [77] **Dixon T**, Lotz SD, Dickson A. Predicting ligand binding affinity using on-and off-rates for the SAMPL6 SAMPLing
1510 challenge. *Journal of computer-aided molecular design*. 2018; 32(10):1001–1012.
- 1511 [78] **Shirts MR**, Chodera JD. Statistically optimal analysis of samples from multiple equilibrium states. *The Journal of*
1512 *chemical physics*. 2008; 129(12):124105. doi: [10.1063/1.2978177](https://doi.org/10.1063/1.2978177).
- 1513 [79] **Rizzi A**, Chodera J, Naden L, Beauchamp K, Grinaway P, Rustenburg B, Albanese S, Saladi S, choderalab/yank: 0.20.1
1514 - Exact treatment of PME electrostatics and optimizations; 2018. <https://doi.org/10.5281/zenodo.1161274>, doi:
1515 [10.5281/zenodo.1161274](https://doi.org/10.5281/zenodo.1161274).
- 1516 [80] **Wang K**, Chodera JD, Yang Y, Shirts MR. Identifying ligand binding sites and poses using GPU-accelerated Hamiltonian
1517 replica exchange molecular dynamics. *Journal of computer-aided molecular design*. 2013; 27(12):989–1007.
- 1518 [81] **Beutler TC**, Mark AE, van Schaik RC, Gerber PR, Van Gunsteren WF. Avoiding singularities and numerical instabilities
1519 in free energy calculations based on molecular simulations. *Chemical physics letters*. 1994; 222(6):529–539.
- 1520 [82] **Chodera JD**, Shirts MR. Replica exchange and expanded ensemble simulations as Gibbs sampling: Simple improve-
1521 ments for enhanced mixing. *The Journal of chemical physics*. 2011; 135(19):194110.
- 1522 [83] **Desgranges C**, Delhommelle J. Evaluation of the grand-canonical partition function using expanded Wang-Landau
1523 simulations. I. Thermodynamic properties in the bulk and at the liquid-vapor phase boundary. *The Journal of*
1524 *Chemical Physics*. 2012; 136(18):184107.
- 1525 [84] **Wang F**, Landau D. Efficient, multiple-range random walk algorithm to calculate the density of states. *Physical*
1526 *review letters*. 2001; 86(10):2050.
- 1527 [85] **Woods CJ**, Mey AS, Calabro G, Julien M, Sire molecular simulation framework;. <https://siremol.org>.
- 1528 [86] **Andersen HC**. Molecular dynamics simulations at constant pressure and/or temperature. *The Journal of chemical*
1529 *physics*. 1980; 72(4):2384–2393.
- 1530 [87] **Tironi IG**, Sperb R, Smith PE, van Gunsteren WF. A generalized reaction field method for molecular dynamics
1531 simulations. *The Journal of chemical physics*. 1995; 102(13):5451–5459.
- 1532 [88] **Barker J**, Watts R. Monte Carlo studies of the dielectric properties of water-like models. *Molecular Physics*. 1973;
1533 26(3):789–792.
- 1534 [89] **Bernardi R**, Bhandarkar M, Bhatle BA A, Brunner R, Buelens F, Chipot C, Dalke A, Dixit S, Fiorin G, Freddolino P,
1535 Fu H, Grayson P, Gullingsrud J, Gursoy A, Hardy D, Harrison C, Hénin J, Humphrey W, Hurwitz D, Hynninen A, et al.
1536 NAMD User's Guide. Version 2.12;.
- 1537 [90] **Gapsys V**, Michielssens S, Peters JH, de Groot BL, Leonov H. Calculation of binding free energies. In: *Molecular*
1538 *Modeling of Proteins* Springer; 2015.p. 173–209.
- 1539 [91] **Boresch S**, Tettinger F, Leitgeb M, Karplus M. Absolute binding free energies: a quantitative approach for their
1540 calculation. *The Journal of Physical Chemistry B*. 2003; 107(35):9535–9551. doi: [10.1021/jp0217839](https://doi.org/10.1021/jp0217839).
- 1541 [92] **Crooks GE**. Entropy production fluctuation theorem and the nonequilibrium work relation for free energy differ-
1542 ences. *Physical Review E*. 1999; 60(3):2721.
- 1543 [93] **Velez-Vega C**, Gilson MK. Overcoming dissipation in the calculation of standard binding free energies by ligand
1544 extraction. *Journal of computational chemistry*. 2013; 34(27):2360–2371.
- 1545 [94] **Henriksen NM**, Fenley AT, Gilson MK. Computational calorimetry: high-precision calculation of host-guest binding
1546 thermodynamics. *Journal of chemical theory and computation*. 2015; 11(9):4377–4394.

- 1547 [95] **Donyapour N**, Roussey NM, Dickson A. REVO: Resampling of ensembles by variation optimization. *Journal of*
1548 *Chemical Physics*. 2019; 150:244112.
- 1549 [96] **Essmann U**, Perera L, Berkowitz ML, Darden T, Lee H, Pedersen LG. A smooth particle mesh Ewald method. *The*
1550 *Journal of chemical physics*. 1995; 103(19):8577–8593. doi: [10.1063/1.470117](https://doi.org/10.1063/1.470117).
- 1551 [97] **You W**, Tang Z, Chang CeA. Potential mean force from umbrella sampling simulations: what can we learn and what
1552 is missed? *Journal of chemical theory and computation*. 2019; 15(4):2433–2443.
- 1553 [98] **Laury ML**, Wang Z, Gordon AS, Ponder JW. Absolute binding free energies for the SAMPL6 cucurbit [8] uril
1554 host-guest challenge via the AMOEBA polarizable force field. *Journal of computer-aided molecular design*. 2018;
1555 32(10):1087–1095.
- 1556 [99] **Efron B**. Better bootstrap confidence intervals. *Journal of the American statistical Association*. 1987; 82(397):171–
1557 185.
- 1558 [100] **Monroe JI**, Shirts MR. Converging free energies of binding in cucurbit [7] uril and octa-acid host-guest systems from
1559 SAMPL4 using expanded ensemble simulations. *Journal of computer-aided molecular design*. 2014; 28(4):401–415.
- 1560 [101] **Crooks GE**. Path-ensemble averages in systems driven far from equilibrium. *Physical review E*. 2000; 61(3):2361.
- 1561 [102] **Hummer G**. Fast-growth thermodynamic integration: Error and efficiency analysis. *The Journal of Chemical Physics*.
1562 2001; 114(17):7330–7337.
- 1563 [103] **Jarzynski C**. Nonequilibrium equality for free energy differences. *Physical Review Letters*. 1997; 78(14):2690.
- 1564 [104] **Chow KH**, Ferguson DM. Isothermal-isobaric molecular dynamics simulations with Monte Carlo volume sampling.
1565 *Computer physics communications*. 1995; 91(1-3):283–289.
- 1566 [105] **Åqvist J**, Wennerström P, Nervall M, Bjelic S, Brandsdal BO. Molecular dynamics simulations of water and
1567 biomolecules with a Monte Carlo constant pressure algorithm. *Chemical physics letters*. 2004; 384(4-6):288–294.
- 1568 [106] **Berendsen HJ**, Postma Jv, van Gunsteren WF, DiNola A, Haak J. Molecular dynamics with coupling to an external
1569 bath. *The Journal of chemical physics*. 1984; 81(8):3684–3690.
- 1570 [107] **Merz PT**, Shirts MR. Testing for physical validity in molecular simulations. *PloS one*. 2018; 13(9):e0202764.
- 1571 [108] **Shirts MR**. Simple quantitative tests to validate sampling from thermodynamic ensembles. *Journal of chemical*
1572 *theory and computation*. 2013; 9(2):909–926.
- 1573 [109] **Lehmann EL**, Casella G. *Theory of point estimation*. Springer Science & Business Media; 2006.
- 1574 [110] **Chodera JD**, Mobley DL. Entropy-Enthalpy Compensation: Role and Ramifications in Biomolecular Lig-
1575 and Recognition and Design. *Annual Review of Biophysics*. 2013; 42(1):121–142. [https://doi.org/10.1146/](https://doi.org/10.1146/annurev-biophys-083012-130318)
1576 [annurev-biophys-083012-130318](https://doi.org/10.1146/annurev-biophys-083012-130318), doi: [10.1146/annurev-biophys-083012-130318](https://doi.org/10.1146/annurev-biophys-083012-130318), PMID: 23654303.
- 1577 [111] **Chodera JD**, Swope WC, Pitera JW, Seok C, Dill KA. Use of the weighted histogram analysis method for the analysis
1578 of simulated and parallel tempering simulations. *Journal of Chemical Theory and Computation*. 2007; 3(1):26–41.
- 1579 [112] **Murkli S**, McNeill JN, Isaacs L. Cucurbit [8] uril• guest complexes: blinded dataset for the SAMPL6 challenge.
1580 *Supramolecular Chemistry*. 2019; 31(3):150–158.
- 1581 [113] **Sullivan MR**, Yao W, Gibb BC. The thermodynamics of guest complexation to octa-acid and tetra-endo-methyl
1582 octa-acid: reference data for the sixth statistical assessment of modeling of proteins and ligands (SAMPL6).
1583 *Supramolecular Chemistry*. 2019; 31(3):184–189.
- 1584 [114] **Pohorille A**, Jarzynski C, Chipot C. Good practices in free-energy calculations. *The Journal of Physical Chemistry B*.
1585 2010; 114(32):10235–10253.
- 1586 [115] **Grossfield A**, Patrone PN, Roe DR, Schultz AJ, Siderius DW, Zuckerman DM. Best practices for quantification of
1587 uncertainty and sampling quality in molecular simulations [Article v1. 0]. *Living journal of computational molecular*
1588 *science*. 2018; 1(1).
- 1589 [116] **Bhati AP**, Wan S, Hu Y, Sherborne B, Coveney PV. Uncertainty quantification in alchemical free energy methods.
1590 *Journal of chemical theory and computation*. 2018; 14(6):2867–2880.
- 1591 [117] **Balasubramanian V**, Jensen T, Turilli M, Kasson P, Shirts M, Jha S. Adaptive Ensemble Biomolecular Simulations at
1592 Scale. *arXiv preprint arXiv:180404736*. 2018; .

- 1593 [118] **Wang L**, Berne B, Friesner RA. On achieving high accuracy and reliability in the calculation of relative protein–ligand
1594 binding affinities. *Proceedings of the National Academy of Sciences*. 2012; 109(6):1937–1942.
- 1595 [119] **Shelley JC**, Cholleti A, Frye LL, Greenwood JR, Timlin MR, Uchimaya M. Epik: a software program for pK_a prediction
1596 and protonation state generation for drug-like molecules. *Journal of computer-aided molecular design*. 2007;
1597 21(12):681–691. doi: [10.1007/s10822-007-9133-z](https://doi.org/10.1007/s10822-007-9133-z).
- 1598 [120] **Greenwood JR**, Calkins D, Sullivan AP, Shelley JC. Towards the comprehensive, rapid, and accurate prediction of
1599 the favorable tautomeric states of drug-like molecules in aqueous solution. *Journal of computer-aided molecular
1600 design*. 2010; 24(6-7):591–604. doi: [10.1007/s10822-010-9349-1](https://doi.org/10.1007/s10822-010-9349-1).
- 1601 [121] **Wang J**, Wang W, Kollman PA, Case DA. Automatic atom type and bond type perception in molecular mechanical
1602 calculations. *Journal of molecular graphics and modelling*. 2006; 25(2):247–260.
- 1603 [122] **Case D**, Betz R, Cerutti D, Cheatham T, III, Darden T, Duke R, Giese T, Gohlke H, Goetz A, Homeyer N, Izadi S, Janowski
1604 P, Kaus J, Kovalenko A, Lee T, LeGrand S, Li P, Lin C, Luchko T, et al., AMBER 16; 2016. University of California, San
1605 Francisco.
- 1606 [123] **Joung IS**, Cheatham III TE. Determination of alkali and halide monovalent ion parameters for use in explicitly
1607 solvated biomolecular simulations. *The journal of physical chemistry B*. 2008; 112(30):9020–9041.
- 1608 [124] **Chodera J**, Rizzi A, Naden L, Beauchamp K, Grinaway P, Fass J, Rustenburg B, Ross GA, Simmonett A, Swenson DWH,
1609 choderalab/openmmtools: 0.14.0 - Exact treatment of alchemical PME electrostatics, water cluster test system,
1610 optimizations; 2018. <https://doi.org/10.5281/zenodo.1161149>, doi: [10.5281/zenodo.1161149](https://doi.org/10.5281/zenodo.1161149).
- 1611 [125] **McGibbon RT**, Beauchamp KA, Harrigan MP, Klein C, Swails JM, Hernández CX, Schwantes CR, Wang LP, Lane TJ,
1612 Pande VS. MDTraj: A Modern Open Library for the Analysis of Molecular Dynamics Trajectories. *Biophysical Journal*.
1613 2015; 109(8):1528 – 1532. doi: [10.1016/j.bpj.2015.08.015](https://doi.org/10.1016/j.bpj.2015.08.015).
- 1614 [126] **Parrinello M**, Rahman A. Crystal structure and pair potentials: A molecular-dynamics study. *Physical Review Letters*.
1615 1980; 45(14):1196.
- 1616 [127] **Gapsys V**, Michielssens S, Seeliger D, de Groot BL. pmx: Automated protein structure and topology generation for
1617 alchemical perturbations. *Journal of computational chemistry*. 2015; 36(5):348–354.
- 1618 [128] **Bennett CH**. Efficient estimation of free energy differences from Monte Carlo data. *Journal of Computational
1619 Physics*. 1976; 22(2):245–268. doi: [10.1016/0021-9991\(76\)90078-4](https://doi.org/10.1016/0021-9991(76)90078-4).
- 1620 [129] **Shirts MR**, Bair E, Hooker G, Pande VS. Equilibrium free energies from nonequilibrium measurements using
1621 maximum-likelihood methods. *Physical review letters*. 2003; 91(14):140601.
- 1622 [130] **Feller SE**, Zhang Y, Pastor RW, Brooks BR. Constant pressure molecular dynamics simulation: the Langevin piston
1623 method. *The Journal of chemical physics*. 1995; 103(11):4613–4621.
- 1624 [131] **Jakobsen AF**. Constant-pressure and constant-surface tension simulations in dissipative particle dynamics. *The
1625 Journal of chemical physics*. 2005; 122(12):124901.
- 1626 [132] **Liu P**, Dehez F, Cai W, Chipot C. A toolkit for the analysis of free-energy perturbation calculations. *Journal of
1627 chemical theory and computation*. 2012; 8(8):2606–2616.
- 1628 [133] **Chodera JD**. A simple method for automated equilibration detection in molecular simulations. *Journal of chemical
1629 theory and computation*. 2016; 12(4):1799–1805.
- 1630 [134] **Sheppard K**, Khrapov S, Lipták G, Capellini R, esvhd, Hogle, JPN, RENE-CORAIL X, Rose ME, jbrockmendel, bash-
1631 tage/arch: Release 4.7; 2018. <https://doi.org/10.5281/zenodo.2240590>, doi: [10.5281/zenodo.2240590](https://doi.org/10.5281/zenodo.2240590).